ARMY RESEARCH LABORATORY

# Addendum to ARL-TR-4005
# Adding Weather to Wargames

**by Sean G. O'Brien and Richard C. Shirkey**

**ARL-TR-4460** **May 2008**

## NOTICES

### Disclaimers

The findings in this report are not to be construed as an official Department of the Army position unless so designated by other authorized documents.

Citation of manufacturer's or trade names does not constitute an official endorsement or approval of the use thereof.

Destroy this report when it is no longer needed. Do not return it to the originator.

# Army Research Laboratory
**White Sands Missile Range, NM 88008-5501**

**ARL-TR-4460** **May 2008**


# Addendum to ARL-TR-4005
# Adding Weather to Wargames


**Sean G. O'Brien and Richard C. Shirkey**
**Computational Information Sciences Directorate, ARL**

# REPORT DOCUMENTATION PAGE

*Form Approved*
*OMB No. 0704-0188*



| 1. REPORT DATE *(DD-MM-YYYY)* | 2. REPORT TYPE | 3. DATES COVERED (From - To) |
|---|---|---|
| May 2008 | Final | 2003-2006 |

**4. TITLE AND SUBTITLE**
Addendum to ARL-TR-4005 Adding Weather to Wargames

**5a. CONTRACT NUMBER**

**5b. GRANT NUMBER**

**5c. PROGRAM ELEMENT NUMBER**

**6. AUTHOR(S)**
Sean G. O'Brien and Richard C. Shirkey

**5d. PROJECT NUMBER**

**5e. TASK NUMBER**

**5f. WORK UNIT NUMBER**

**7. PERFORMING ORGANIZATION NAME(S) AND ADDRESS(ES)**
U.S. Army Research Laboratory
Computational and Information Sciences Directorate
Battlefield Environment Division (ATTN: AMSRD-ARL-CI-EE)
White Sands Missile Range, NM 88002-5501

**8. PERFORMING ORGANIZATION REPORT NUMBER**
ARL-TR-4460

**9. SPONSORING/MONITORING AGENCY NAME(S) AND ADDRESS(ES)**

**10. SPONSOR/MONITOR'S ACRONYM(S)**

**11. SPONSOR/MONITOR'S REPORT NUMBER(S)**

**12. DISTRIBUTION/AVAILABILITY STATEMENT**
Approved for public release; distribution is unlimited.

**13. SUPPLEMENTARY NOTES**

**14. ABSTRACT**
This addendum presents updated graphical representations of the selected Target Acquisition Weapons Software (TAWS) output and also the coefficients for the third order polynomial fits that originally appeared in appendices B and C.

**15. SUBJECT TERMS**
Wargames, weather, sensors, rules, parametric curve fits, target acquisition

| 16. SECURITY CLASSIFICATION OF: | | | 17. LIMITATION OF ABSTRACT | 18. NUMBER OF PAGES | 19a. NAME OF RESPONSIBLE PERSON |
|---|---|---|---|---|---|
| a. REPORT | b. ABSTRACT | c. THIS PAGE | | | Richard C. Shirkey |
| U | U | U | UU | 44 | 19b. TELEPHONE NUMBER (*Include area code*) (575) 678-1570 |

**Standard Form 298 (Rev. 8/98)**
Prescribed by ANSI Std. Z39.1

## Contents

## List of Figures

## List of Tables

## Summary

The method used for calculation of the third order polynomials in the original report "Adding Weather to Wargames" (*1*), did not provide a satisfactory fit in all cases. In addition, we ascertained that some spurious data from the Target Acquisition Weapons Software (TAWS) output were used in the calculation of the parametric curves. Therefore, we have redone the graphs and recalculated the polynomial coefficients for the parametric curves that appeared in appendices B and C using a different technique (*2*). To assure a better fit, we added 3 "synthetic" data points between the 4 normalized detection ranges at visibilities of 0.1, 1.0, 10.0, and 100.0. We assumed that the 4 input data points are evenly spaced in ln space, so that the 3 synthetic points are midway in both ln x and ln y. The polynomial now takes the following form:

$$Ndr = a_0 + a_1 * \ln(V) + a_2 * \ln(V)^2 + a_3 * \ln(V)^3, \quad (1)$$

Where Ndr is the normalized detection range, V is the visibility in km, and $a_0$-$a_3$ are the third order polynomial coefficients.

Appendices B and C have been updated with corrected versions of the graphs for normalized detection range vs. visibility, and with the new third order polynomial coefficients.

## History

Employing the capability of the Target Acquisition Weapons Software (TAWS) tactical decision aid, and the rules embodied in the Integrated Weather Effects Decision Aid (IWEDA) we developed techniques that allowed significant improvement in weather effects and impacts for wargames. TAWS was run for numerous and varied weather conditions; the resultant database was subsequently used to construct third-order polynomial curves to represent infrared sensors acquiring targets under those weather conditions. IWEDA rules were used in determination of go/no-go weather situations for platforms or systems. We found that the wargame realism was increased without impacting the run time. While these techniques are applicable to wargames in general, we tested them by incorporation into the Advanced Warfighting Simulation (AWARS) model. AWARS was modified to incorporate weather impacts upon sensor operation and platform mobility. These modifications included revision of the direct-fire sensor detection algorithm to reflect variations of the maximum number of resolution cycles over the direct fire target with meteorological visibility, time of day, sky cover, target state, and haze aerosol type. The speed of these computations was an important consideration, so the parametric fit technique was selected after a favorable comparison with table look-up methods. Weather effects upon combatant platform mobility were modeled by implementation of IWEDA rules classes for both helicopters and fixed-wing aircraft platforms. The impacts of these modifications in both the presence and absence of adverse weather conditions were tested and are summarized.

## 2. Addendum to Appendices B and C

**A special note about Monikers used in appendices B and C.**

Table A-4 applies to both appendices B and C.

Each moniker, used in the following table, is a concatenation of the various atmospheric conditions that we used; with the exception of the 0900 time period, the first three characters of each atmospheric condition were used. This cipher is presented in table A-4.

Table A-4. Monikers and their meaning as used in the various tables and figures in appendices B and C.

| Moniker | Meaning |
|---|---|
| Fog | Fog |
| Rur | Rural |
| Tan | Tank |
| Exe | Exercised |
| Off | Inactive |
| 900 | 0900 |
| 150 | 1500 |
| Win | Winter |

Table A-4. Monikers and their meaning as used in the various tables and figures in appendices B and C (continued).

| **Moniker** | **Meaning** |
|---|---|
| Sum | Summer |
| Nor | North |
| Sou | South |
| Eas | East |
| Wes | West |
| Ove | Overcast |
| Cle | Clear |

# Appendix B. Third-Order Polynomial Coefficients and their Curves for the Fog Aerosol for a Narrow Field of View (NFOV) and Wide Field of View (WFOV) Average Infrared (IR) Sensor

Table B-1. Third-order polynomial coefficients curve fit to averaged quantities as represented by moniker for average sensor viewing through a fog aerosol. WFOV results are shown.

| Moniker | a0 | a1 | a2 | a3 | Average Maximum Detection Range |
|---|---|---|---|---|---|
| 150CleFog | 0.7182 | 0.1504 | -0.0111 | -0.0018 | 3.59 |
| 150OveFog | 0.7051 | 0.1536 | -0.0098 | -0.0021 | 3.59 |
| 900CleFog | 0.6241 | 0.1648 | -0.0022 | -0.0034 | 3.42 |
| 900OveFog | 0.5536 | 0.1661 | 0.0036 | -0.0041 | 3.25 |
| Tan900CleFog | 0.7090 | 0.1455 | -0.0100 | -0.0017 | 2.69 |
| Tan150CleFog | 0.8033 | 0.1232 | -0.0185 | 0.0002 | 2.80 |
| Tan900OveFog | 0.6682 | 0.1527 | -0.0063 | -0.0024 | 2.68 |
| Tan150OveFog | 0.7953 | 0.1260 | -0.0180 | 0.0001 | 2.79 |
| TanExe150OveFog | 0.8185 | 0.1193 | -0.0205 | 0.0007 | 2.82 |
| TanExe900OveFog | 0.7568 | 0.1391 | -0.0147 | -0.0009 | 2.78 |
| TanExe150CleFog | 0.8193 | 0.1183 | -0.0201 | 0.0006 | 2.82 |
| TanExe900CleFog | 0.7667 | 0.1352 | -0.0152 | -0.0007 | 2.78 |
| TanOff900CleFog | 0.6369 | 0.1580 | -0.0036 | -0.0029 | 2.58 |
| TanOff150CleFog | 0.7872 | 0.1281 | -0.0170 | -0.0002 | 2.78 |
| TanOff150OveFog | 0.7722 | 0.1327 | -0.0155 | -0.0006 | 2.76 |
| TanOff900OveFog | 0.5662 | 0.1674 | 0.0032 | -0.0041 | 2.56 |
| TanOff900SumOveFog | 0.5723 | 0.1665 | 0.0023 | -0.0040 | 2.45 |
| TanOff900WinOveFog | 0.5351 | 0.1712 | 0.0062 | -0.0047 | 2.63 |
| TanOff150SumOveFog | 0.7868 | 0.1275 | -0.0167 | -0.0002 | 2.77 |
| TanOff150WinOveFog | 0.7284 | 0.1484 | -0.0124 | -0.0015 | 2.74 |
| TanOff900NorOveFog | 0.5555 | 0.1648 | 0.0034 | -0.0040 | 2.51 |
| TanOff900EasOveFog | 0.5345 | 0.1637 | 0.0061 | -0.0043 | 2.44 |
| TanOff900WesOveFog | 0.6175 | 0.1712 | -0.0007 | -0.0040 | 2.66 |
| TanOff900SouOveFog | 0.5486 | 0.1688 | 0.0043 | -0.0043 | 2.60 |
| TanExe900SumOveFog | 0.7575 | 0.1385 | -0.0146 | -0.0009 | 2.78 |
| TanExe900WinOveFog | 0.7517 | 0.1415 | -0.0144 | -0.0010 | 2.79 |
| TanExe150SumOveFog | 0.8231 | 0.1169 | -0.0207 | 0.0008 | 2.81 |
| TanExe150WinOveFog | 0.8012 | 0.1265 | -0.0193 | 0.0003 | 2.81 |
| TanExe900NorOveFog | 0.8309 | 0.1168 | -0.0220 | 0.0010 | 2.85 |
| TanExe900EasOveFog | 0.7412 | 0.1441 | -0.0134 | -0.0012 | 2.76 |
| TanExe900WesOveFog | 0.7599 | 0.1393 | -0.0159 | -0.0007 | 2.80 |
| TanExe900SouOveFog | 0.6952 | 0.1557 | -0.0077 | -0.0026 | 2.72 |
| TanExe150NorOveFog | 0.8464 | 0.1112 | -0.0232 | 0.0014 | 2.85 |
| TanExe150EasOveFog | 0.8219 | 0.1179 | -0.0208 | 0.0008 | 2.81 |
| TanExe150WesOveFog | 0.8185 | 0.1193 | -0.0207 | 0.0007 | 2.83 |
| TanExe150SouOveFog | 0.7870 | 0.1287 | -0.0173 | -0.0001 | 2.78 |

Table B-1. Third-order polynomial coefficients curve fit to averaged quantities as represented by moniker for average sensor viewing through a fog aerosol. WFOV results are shown (continued).

| Moniker | a0 | a1 | a2 | a3 | Average Maximum Detection Range |
|---|---|---|---|---|---|
| TanExe900NorCleFog | 0.8335 | 0.1162 | -0.0223 | 0.0011 | 2.85 |
| TanExe900EasCleFog | 0.7429 | 0.1444 | -0.0140 | -0.0011 | 2.76 |
| TanExe900WesCleFog | 0.8014 | 0.1232 | -0.0179 | 0.0001 | 2.81 |
| TanExe900SouCleFog | 0.6892 | 0.1565 | -0.0067 | -0.0027 | 2.72 |
| TanExe150NorCleFog | 0.8514 | 0.1092 | -0.0234 | 0.0015 | 2.85 |
| TanExe150EasCleFog | 0.8345 | 0.1130 | -0.0214 | 0.0010 | 2.83 |
| TanExe150WesCleFog | 0.8071 | 0.1221 | -0.0189 | 0.0003 | 2.80 |
| TanExe150SouCleFog | 0.7842 | 0.1287 | -0.0166 | -0.0003 | 2.79 |
| TanOff900NorCleFog | 0.6124 | 0.1661 | -0.0014 | -0.0035 | 2.49 |
| TanOff900EasCleFog | 0.5519 | 0.1665 | 0.0043 | -0.0042 | 2.40 |
| TanOff900WesCleFog | 0.7673 | 0.1361 | -0.0163 | -0.0005 | 2.77 |
| TanOff900SouCleFog | 0.5699 | 0.1695 | 0.0030 | -0.0042 | 2.59 |
| TanOff150NorCleFog | 0.7812 | 0.1296 | -0.0161 | -0.0004 | 2.77 |
| TanOff150EasCleFog | 0.8207 | 0.1188 | -0.0211 | 0.0008 | 2.80 |
| TanOff150WesCleFog | 0.7811 | 0.1300 | -0.0164 | -0.0003 | 2.77 |
| TanOff150SouCleFog | 0.7657 | 0.1339 | -0.0144 | -0.0008 | 2.76 |
| TanOff900SumNorCleFog | 0.5304 | 0.1487 | 0.0030 | -0.0029 | 2.07 |
| TanOff900SumEasCleFog | 0.5475 | 0.1590 | 0.0016 | -0.0032 | 2.58 |
| TanOff900SumWesCleFog | 0.7699 | 0.1366 | -0.0174 | -0.0003 | 2.78 |
| TanOff900SumSouCleFog | 0.5875 | 0.1760 | 0.0021 | -0.0045 | 2.70 |
| TanOff150SumNorCleFog | 0.7726 | 0.1317 | -0.0150 | -0.0006 | 2.75 |
| TanOff150SumEasCleFog | 0.8275 | 0.1168 | -0.0220 | 0.0010 | 2.80 |
| TanOff150SumWesCleFog | 0.7937 | 0.1252 | -0.0173 | 0.0000 | 2.78 |
| TanOff150SumSouCleFog | 0.7975 | 0.1246 | -0.0179 | 0.0001 | 2.78 |
| TanOff900WinNorCleFog | 0.6554 | 0.1679 | -0.0042 | -0.0035 | 2.72 |
| TanOff90Win0EasCleFog | 0.6038 | 0.1802 | 0.0008 | -0.0046 | 2.69 |
| TanOff900WinWesCleFog | 0.7554 | 0.1429 | -0.0166 | -0.0006 | 2.77 |
| TanOff900WinSouCleFog | 0.5575 | 0.1651 | 0.0033 | -0.0040 | 2.78 |
| TanOff150WinNorCleFog | 0.7845 | 0.1301 | -0.0171 | -0.0002 | 2.81 |
| TanOff150WinEasCleFog | 0.8006 | 0.1248 | -0.0183 | 0.0001 | 2.79 |
| TanOff150WinWesCleFog | 0.7419 | 0.1449 | -0.0138 | -0.0012 | 2.75 |
| TanOff150WinSouCleFog | 0.6910 | 0.1564 | -0.0070 | -0.0027 | 2.74 |
| TanExe900SumNorCleFog | 0.8276 | 0.1173 | -0.0214 | 0.0009 | 2.85 |
| TanExe900SumEasCleFog | 0.7327 | 0.1466 | -0.0125 | -0.0015 | 2.75 |
| TanExe900SumWesCleFog | 0.8008 | 0.1229 | -0.0176 | 0.0001 | 2.81 |
| TanExe900SumSouCleFog | 0.7083 | 0.1520 | -0.0091 | -0.0022 | 2.74 |
| TanExe150SumNorCleFog | 0.8498 | 0.1091 | -0.0234 | 0.0015 | 2.85 |
| TanExe150SumEasCleFog | 0.8344 | 0.1121 | -0.0209 | 0.0009 | 2.82 |
| TanExe150SumWesCleFog | 0.8090 | 0.1212 | -0.0191 | 0.0004 | 2.80 |
| TanExe150SumSouCleFog | 0.8009 | 0.1223 | -0.0177 | 0.0001 | 2.80 |
| TanExe900WinNorCleFog | 0.8514 | 0.1138 | -0.0250 | 0.0016 | 2.85 |
| TanExe90Win0EasCleFog | 0.7675 | 0.1396 | -0.0177 | -0.0004 | 2.78 |
| TanExe900WinWesCleFog | 0.8006 | 0.1249 | -0.0183 | 0.0001 | 2.82 |

Table B-1. Third-order polynomial coefficients curve fit to averaged quantities as represented by moniker for average sensor viewing through a fog aerosol. WFOV results are shown (continued).

| Moniker | a0 | a1 | a2 | a3 | Average Maximum Detection Range |
|---|---|---|---|---|---|
| TanExe900WinSouCleFog | 0.6819 | 0.1585 | -0.0060 | -0.0029 | 2.75 |
| TanExe150WinNorCleFog | 0.8608 | 0.1096 | -0.0251 | 0.0017 | 2.85 |
| TanExe150WinEasCleFog | 0.8311 | 0.1164 | -0.0221 | 0.0010 | 2.85 |
| TanExe150WinWesCleFog | 0.8003 | 0.1249 | -0.0183 | 0.0001 | 2.81 |
| TanExe150WinSouCleFog | 0.7350 | 0.1463 | -0.0130 | -0.0014 | 2.76 |
| TanOff900SumNorOveFog | 0.5525 | 0.1583 | 0.0030 | -0.0035 | 2.01 |
| TanOff900SumEasOveFog | 0.5162 | 0.1608 | 0.0080 | -0.0044 | 2.28 |
| TanOff900SumWesOveFog | 0.6465 | 0.1725 | -0.0044 | -0.0036 | 2.67 |
| TanOff900SumSouOveFog | 0.5421 | 0.1674 | 0.0051 | -0.0043 | 2.53 |
| TanOff150SumNorOveFog | 0.7724 | 0.1328 | -0.0156 | -0.0005 | 2.74 |
| TanOff150SumEasOveFog | 0.8011 | 0.1230 | -0.0180 | 0.0001 | 2.78 |
| TanOff150SumWesOveFog | 0.8003 | 0.1237 | -0.0182 | 0.0002 | 2.78 |
| TanOff150SumSouOveFog | 0.7734 | 0.1307 | -0.0148 | -0.0006 | 2.76 |
| TanOff900WinNorOveFog | 0.5529 | 0.1669 | 0.0035 | -0.0040 | 2.69 |
| TanOff900Win0EasOveFo | 0.5323 | 0.1726 | 0.0073 | -0.0049 | 2.53 |
| TanOff900WinWesOveFog | 0.5287 | 0.1738 | 0.0080 | -0.0051 | 2.62 |
| TanOff900WinSouOveFog | 0.5308 | 0.1692 | 0.0045 | -0.0042 | 2.74 |
| TanOff150WinNorOveFog | 0.7340 | 0.1479 | -0.0137 | -0.0013 | 2.74 |
| TanOff150WinEasOveFog | 0.7421 | 0.1448 | -0.0139 | -0.0012 | 2.74 |
| TanOff150WinWesOveFog | 0.7381 | 0.1459 | -0.0134 | -0.0013 | 2.74 |
| TanOff150WinSouOveFog | 0.6992 | 0.1547 | -0.0085 | -0.0024 | 2.73 |
| TanExe900SumNorOveFog | 0.8276 | 0.1173 | -0.0214 | 0.0009 | 2.85 |
| TanExe900SumEasOveFog | 0.7380 | 0.1453 | -0.0135 | -0.0012 | 2.77 |
| TanExe900SumWesOveFog | 0.7713 | 0.1347 | -0.0165 | -0.0004 | 2.78 |
| TanExe900SumSouOveFog | 0.6931 | 0.1563 | -0.0073 | -0.0027 | 2.71 |
| TanExe150SumNorOveFog | 0.8420 | 0.1112 | -0.0224 | 0.0012 | 2.85 |
| TanExe150SumEasOveFog | 0.8283 | 0.1157 | -0.0215 | 0.0010 | 2.81 |
| TanExe150SumWesOveFog | 0.8244 | 0.1167 | -0.0210 | 0.0009 | 2.81 |
| TanExe150SumSouOveFog | 0.7978 | 0.1241 | -0.0178 | 0.0001 | 2.78 |
| TanExe900WinNorOveFog | 0.8411 | 0.1163 | -0.0235 | 0.0012 | 2.85 |
| TanExe900WinEasOveFog | 0.7405 | 0.1454 | -0.0138 | -0.0012 | 2.78 |
| TanExe900WinWesOveFog | 0.7405 | 0.1454 | -0.0138 | -0.0012 | 2.78 |
| TanExe900WinSouOveFog | 0.6846 | 0.1585 | -0.0064 | -0.0029 | 2.75 |
| TanExe150WinNorOveFog | 0.8516 | 0.1133 | -0.0247 | 0.0015 | 2.85 |
| TanExe150WinEasOveFog | 0.8029 | 0.1242 | -0.0188 | 0.0002 | 2.81 |
| TanExe150WinWesOveFog | 0.8003 | 0.1249 | -0.0183 | 0.0001 | 2.81 |
| TanExe150WinSouOveFog | 0.7500 | 0.1433 | -0.0153 | -0.0009 | 2.77 |

Table B-2. Third-order polynomial coefficients curve fit to averaged quantities as represented by moniker for average sensor viewing through a fog aerosol. NFOV results are shown. Coefficients in blue have associated curves presented in the graphs in this appendix.

| Moniker | a0 | a1 | a2 | a3 | Average Maximum Detection Range |
|---|---|---|---|---|---|
| 150CleFog | 0.3553 | 0.2145 | 0.0247 | -0.0089 | 8.88 |
| 150OveFog | 0.3459 | 0.2124 | 0.0252 | -0.0088 | 8.88 |
| 900CleFog | 0.3014 | 0.1968 | 0.0262 | -0.0078 | 8.52 |
| 900OveFog | 0.2704 | 0.1762 | 0.0251 | -0.0063 | 8.22 |
| Tan900CleFog | 0.3469 | 0.2067 | 0.0237 | -0.0082 | 7.59 |
| Tan150CleFog | 0.4111 | 0.2204 | 0.0205 | -0.0088 | 7.80 |
| Tan900OveFog | 0.3241 | 0.1972 | 0.0240 | -0.0076 | 7.62 |
| Tan150OveFog | 0.4026 | 0.2206 | 0.0214 | -0.0089 | 7.80 |
| TanExe150OveFog | 0.4226 | 0.2205 | 0.0192 | -0.0087 | 7.80 |
| TanExe900OveFog | 0.3759 | 0.2189 | 0.0232 | -0.0089 | 7.80 |
| TanExe150CleFog | 0.4285 | 0.2201 | 0.0187 | -0.0086 | 7.80 |
| TanExe900CleFog | 0.3835 | 0.2185 | 0.0224 | -0.0088 | 7.80 |
| TanOff900CleFog | 0.3008 | 0.1909 | 0.0251 | -0.0073 | 7.32 |
| TanOff150CleFog | 0.3936 | 0.2203 | 0.0223 | -0.0090 | 7.80 |
| TanOff150OveFog | 0.3824 | 0.2202 | 0.0234 | -0.0091 | 7.80 |
| TanOff900OveFog | 0.2612 | 0.1697 | 0.0249 | -0.0058 | 7.39 |
| TanOff900SumOveFog | 0.2613 | 0.1694 | 0.0248 | -0.0058 | 7.20 |
| TanOff900WinOveFog | 0.2451 | 0.1715 | 0.0267 | -0.0061 | 8.02 |
| TanOff150SumOveFog | 0.3904 | 0.2187 | 0.0226 | -0.0090 | 7.80 |
| TanOff150WinOveFog | 0.3536 | 0.2228 | 0.0261 | -0.0095 | 7.80 |
| TanOff900NorOveFog | 0.2510 | 0.1652 | 0.0247 | -0.0055 | 7.30 |
| TanOff900EasOveFog | 0.2568 | 0.1647 | 0.0244 | -0.0054 | 7.02 |
| TanOff900WesOveFog | 0.2774 | 0.1803 | 0.0255 | -0.0066 | 7.80 |
| TanOff900SouOveFog | 0.2546 | 0.1658 | 0.0247 | -0.0055 | 7.36 |
| TanExe900SumOveFog | 0.3758 | 0.2195 | 0.0234 | -0.0090 | 7.80 |
| TanExe900WinOveFog | 0.3827 | 0.2236 | 0.0230 | -0.0092 | 7.80 |
| TanExe150SumOveFog | 0.4251 | 0.2197 | 0.0191 | -0.0086 | 7.80 |
| TanExe150WinOveFog | 0.4138 | 0.2226 | 0.0198 | -0.0088 | 7.80 |
| TanExe900NorOveFog | 0.4352 | 0.2208 | 0.0176 | -0.0084 | 7.80 |
| TanExe900EasOveFog | 0.3677 | 0.2209 | 0.0243 | -0.0092 | 7.80 |
| TanExe900WesOveFog | 0.3761 | 0.2218 | 0.0238 | -0.0092 | 7.80 |
| TanExe900SouOveFog | 0.3237 | 0.2086 | 0.0264 | -0.0086 | 7.80 |
| TanExe150NorOveFog | 0.4503 | 0.2187 | 0.0162 | -0.0082 | 7.80 |
| TanExe150EasOveFog | 0.4280 | 0.2209 | 0.0186 | -0.0086 | 7.80 |
| TanExe150WesOveFog | 0.4203 | 0.2207 | 0.0196 | -0.0087 | 7.80 |
| TanExe150SouOveFog | 0.3916 | 0.2209 | 0.0224 | -0.0090 | 7.80 |
| TanExe900NorCleFog | 0.4362 | 0.2207 | 0.0174 | -0.0084 | 7.80 |
| TanExe900EasCleFog | 0.3601 | 0.2195 | 0.0248 | -0.0092 | 7.80 |
| TanExe900WesCleFog | 0.4152 | 0.2220 | 0.0200 | -0.0088 | 7.80 |
| TanExe900SouCleFog | 0.3213 | 0.2073 | 0.0266 | -0.0086 | 7.80 |
| TanExe150NorCleFog | 0.4537 | 0.2182 | 0.0159 | -0.0081 | 7.80 |
| TanExe150EasCleFog | 0.4446 | 0.2189 | 0.0171 | -0.0083 | 7.80 |

Table B-2. Third-order polynomial coefficients curve fit to averaged quantities as represented by moniker for average sensor viewing through a fog aerosol. NFOV results are shown. Coefficients in blue have associated curves presented in the graphs in this appendix (continued).

| Moniker | a0 | a1 | a2 | a3 | Average Maximum Detection Range |
|---|---|---|---|---|---|
| TanExe150WesCleFog | 0.4190 | 0.2209 | 0.0197 | -0.0087 | 7.80 |
| TanExe150SouCleFog | 0.3963 | 0.2214 | 0.0221 | -0.0090 | 7.80 |
| TanOff900NorCleFog | 0.2752 | 0.1826 | 0.0257 | -0.0067 | 7.10 |
| TanOff900EasCleFog | 0.2638 | 0.1730 | 0.0254 | -0.0061 | 6.79 |
| TanOff900WesCleFog | 0.3784 | 0.2220 | 0.0240 | -0.0093 | 7.80 |
| TanOff900SouCleFog | 0.2566 | 0.1715 | 0.0253 | -0.0059 | 7.36 |
| TanOff150NorCleFog | 0.3854 | 0.2191 | 0.0231 | -0.0090 | 7.80 |
| TanOff150EasCleFog | 0.4215 | 0.2208 | 0.0195 | -0.0087 | 7.80 |
| TanOff150WesCleFog | 0.3898 | 0.2205 | 0.0225 | -0.0090 | 7.80 |
| TanOff150SouCleFog | 0.3775 | 0.2203 | 0.0238 | -0.0092 | 7.80 |
| TanOff900SumNorCleFog | 0.2300 | 0.1521 | 0.0238 | -0.0044 | 6.23 |
| TanOff900SumEasCleFog | 0.2621 | 0.1658 | 0.0228 | -0.0052 | 7.39 |
| TanOff900SumWesCleFog | 0.3780 | 0.2226 | 0.0242 | -0.0094 | 7.80 |
| TanOff900SumSouCleFog | 0.2586 | 0.1748 | 0.0257 | -0.0062 | 7.70 |
| TanOff150SumNorCleFog | 0.3752 | 0.2169 | 0.0240 | -0.0090 | 7.80 |
| TanOff150SumEasCleFog | 0.4249 | 0.2201 | 0.0193 | -0.0087 | 7.80 |
| TanOff150SumWesCleFog | 0.3964 | 0.2191 | 0.0219 | -0.0089 | 7.80 |
| TanOff150SumSouCleFog | 0.3976 | 0.2194 | 0.0218 | -0.0089 | 7.80 |
| TanOff900WinNorCleFog | 0.3070 | 0.2138 | 0.0291 | -0.0093 | 7.80 |
| TanOff90Win0EasCleFog | 0.2742 | 0.1938 | 0.0283 | -0.0078 | 7.80 |
| TanOff900WinWesCleFog | 0.3738 | 0.2238 | 0.0239 | -0.0093 | 7.80 |
| TanOff900WinSouCleFog | 0.2534 | 0.1781 | 0.0264 | -0.0064 | 8.43 |
| TanOff150WinNorCleFog | 0.3937 | 0.2226 | 0.0226 | -0.0092 | 7.80 |
| TanOff150WinEasCleFog | 0.4114 | 0.2225 | 0.0202 | -0.0089 | 7.80 |
| TanOff150WinWesCleFog | 0.3676 | 0.2234 | 0.0248 | -0.0094 | 7.80 |
| TanOff150WinSouCleFog | 0.3277 | 0.2200 | 0.0281 | -0.0096 | 7.80 |
| TanExe900SumNorCleFog | 0.4310 | 0.2214 | 0.0179 | -0.0085 | 7.80 |
| TanExe900SumEasCleFog | 0.3519 | 0.2202 | 0.0255 | -0.0093 | 7.80 |
| TanExe900SumWesCleFog | 0.4141 | 0.2220 | 0.0202 | -0.0088 | 7.80 |
| TanExe900SumSouCleFog | 0.3349 | 0.2170 | 0.0272 | -0.0093 | 7.80 |
| TanExe150SumNorCleFog | 0.4477 | 0.2186 | 0.0168 | -0.0083 | 7.80 |
| TanExe150SumEasCleFog | 0.4443 | 0.2186 | 0.0174 | -0.0084 | 7.80 |
| TanExe150SumWesCleFog | 0.4203 | 0.2203 | 0.0197 | -0.0087 | 7.80 |
| TanExe150SumSouCleFog | 0.4091 | 0.2205 | 0.0208 | -0.0089 | 7.80 |
| TanExe900WinNorCleFog | 0.4553 | 0.2194 | 0.0148 | -0.0080 | 7.80 |
| TanExe90Win0EasCleFog | 0.3801 | 0.2240 | 0.0231 | -0.0092 | 7.80 |
| TanExe900WinWesCleFog | 0.4160 | 0.2225 | 0.0196 | -0.0088 | 7.80 |
| TanExe900WinSouCleFog | 0.3257 | 0.2201 | 0.0284 | -0.0096 | 7.80 |
| TanExe150WinNorCleFog | 0.4675 | 0.2174 | 0.0137 | -0.0078 | 7.80 |
| TanExe150WinEasCleFog | 0.4410 | 0.2201 | 0.0170 | -0.0083 | 7.80 |
| TanExe150WinWesCleFog | 0.4133 | 0.2225 | 0.0200 | -0.0088 | 7.80 |
| TanExe150WinSouCleFog | 0.3655 | 0.2233 | 0.0250 | -0.0094 | 7.80 |
| TanOff900SumNorOveFog | 0.2422 | 0.1588 | 0.0238 | -0.0049 | 6.02 |

Table B-2. Third-order polynomial coefficients curve fit to averaged quantities as represented by moniker for average sensor viewing through a fog aerosol. NFOV results are shown. Coefficients in blue have associated curves presented in the graphs in this appendix (continued).

| Moniker | a0 | a1 | a2 | a3 | Average Maximum Detection Range |
|---|---|---|---|---|---|
| TanOff900SumEasOveFog | 0.2482 | 0.1568 | 0.0232 | -0.0047 | 7.21 |
| TanOff900SumWesOveFog | 0.2877 | 0.1875 | 0.0261 | -0.0072 | 7.80 |
| TanOff900SumSouOveFog | 0.2503 | 0.1628 | 0.0248 | -0.0053 | 7.19 |
| TanOff150SumNorOveFog | 0.3751 | 0.2166 | 0.0240 | -0.0090 | 7.80 |
| TanOff150SumEasOveFog | 0.4091 | 0.2205 | 0.0208 | -0.0089 | 7.80 |
| TanOff150SumWesOveFog | 0.3986 | 0.2199 | 0.0217 | -0.0089 | 7.80 |
| TanOff150SumSouOveFog | 0.3786 | 0.2175 | 0.0237 | -0.0090 | 7.80 |
| TanOff900WinNorOveFog | 0.2425 | 0.1710 | 0.0269 | -0.0061 | 8.58 |
| TanOff900Win0EasOveFo | 0.2395 | 0.1671 | 0.0266 | -0.0058 | 7.66 |
| TanOff900WinWesOveFog | 0.2470 | 0.1738 | 0.0267 | -0.0062 | 7.79 |
| TanOff900WinSouOveFog | 0.2541 | 0.1755 | 0.0264 | -0.0063 | 8.43 |
| TanOff150WinNorOveFog | 0.3530 | 0.2228 | 0.0262 | -0.0096 | 7.80 |
| TanOff150WinEasOveFog | 0.3670 | 0.2234 | 0.0248 | -0.0094 | 7.80 |
| TanOff150WinWesOveFog | 0.3619 | 0.2231 | 0.0255 | -0.0095 | 7.80 |
| TanOff150WinSouOveFog | 0.3324 | 0.2211 | 0.0278 | -0.0096 | 7.80 |
| TanExe900SumNorOveFog | 0.4335 | 0.2207 | 0.0179 | -0.0085 | 7.80 |
| TanExe900SumEasOveFog | 0.3658 | 0.2219 | 0.0247 | -0.0093 | 7.80 |
| TanExe900SumWesOveFog | 0.3799 | 0.2227 | 0.0239 | -0.0093 | 7.80 |
| TanExe900SumSouOveFog | 0.3230 | 0.2090 | 0.0265 | -0.0086 | 7.80 |
| TanExe150SumNorOveFog | 0.4461 | 0.2188 | 0.0169 | -0.0083 | 7.80 |
| TanExe150SumEasOveFog | 0.4326 | 0.2201 | 0.0182 | -0.0085 | 7.80 |
| TanExe150SumWesOveFog | 0.4230 | 0.2199 | 0.0195 | -0.0087 | 7.80 |
| TanExe150SumSouOveFog | 0.3985 | 0.2194 | 0.0216 | -0.0089 | 7.80 |
| TanExe900WinNorOveFog | 0.4499 | 0.2200 | 0.0154 | -0.0081 | 7.80 |
| TanExe900WinEasOveFog | 0.3771 | 0.2239 | 0.0235 | -0.0093 | 7.80 |
| TanExe900WinWesOveFog | 0.3752 | 0.2238 | 0.0238 | -0.0093 | 7.80 |
| TanExe900WinSouOveFog | 0.3266 | 0.2202 | 0.0283 | -0.0096 | 7.80 |
| TanExe150WinNorOveFog | 0.4595 | 0.2192 | 0.0142 | -0.0079 | 7.80 |
| TanExe150WinEasOveFog | 0.4160 | 0.2225 | 0.0196 | -0.0088 | 7.80 |
| TanExe150WinWesOveFog | 0.4123 | 0.2225 | 0.0201 | -0.0088 | 7.80 |
| TanExe150WinSouOveFog | 0.3666 | 0.2234 | 0.0249 | -0.0094 | 7.80 |

The coefficients displayed in blue in table B-2 have associated curves that are presented in the following graphs labeled figures B-1 through B-15.

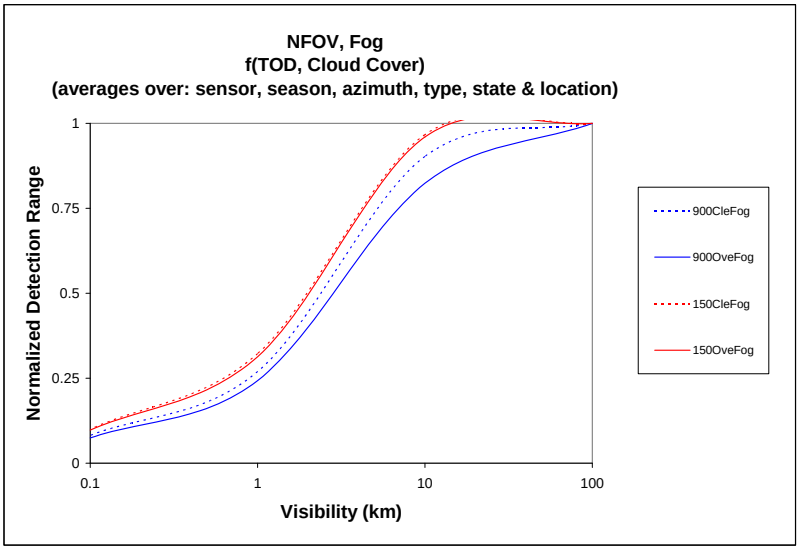


Figure B-1. Normalized detection range vs. visibility for a NFOV average sensor in a fog aerosol as a function of Time of Day (TOD) and, cloud cover. Averages were taken over seasons, locations, azimuths, target types and operating states, as presented in table B-2.

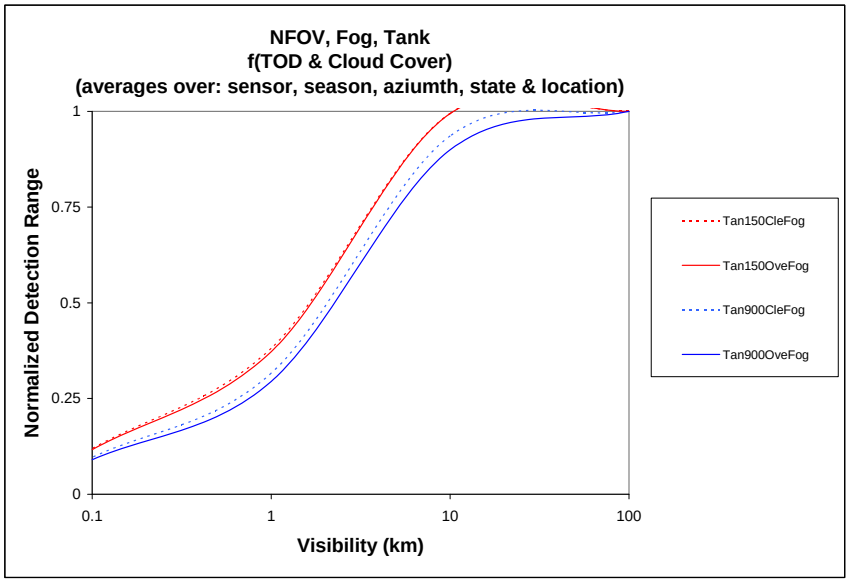


Figure B-2. Normalized detection range vs. visibility for a NFOV average sensor, in a fog aerosol, viewing a tank, as a function of TOD, and cloud cover. Averages were taken over seasons, locations, azimuths, and target operating states, as presented in table B-2.

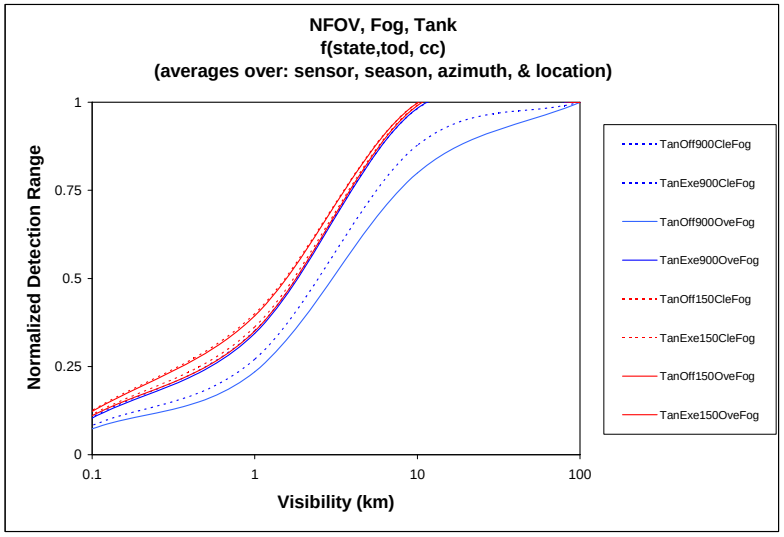


Figure B-3. Normalized detection range vs. visibility for a NFOV average sensor in a fog aerosol as a function of target operating state, TOD, and cloud cover. Averages were taken over seasons, locations, and azimuths, as presented in table B-2.

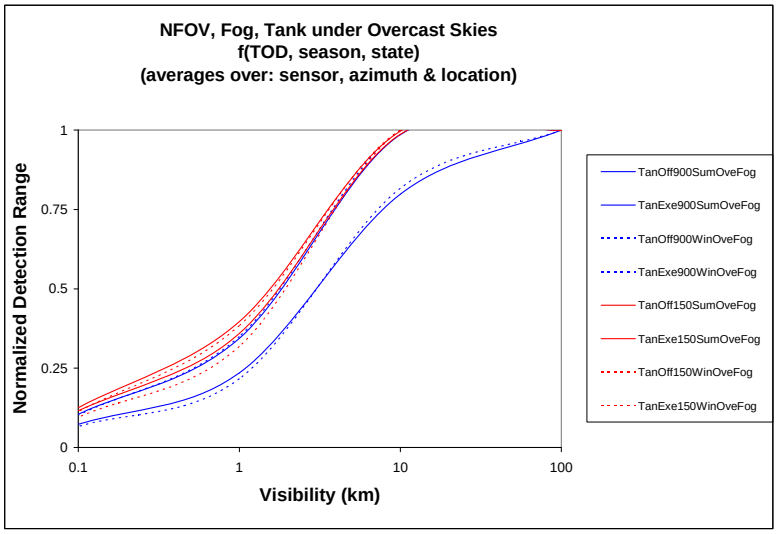


Figure B-4. Normalized detection range vs. visibility for a NFOV average sensor, in a fog aerosol, viewing a tank under overcast skies, as a function of TOD, season, and operating state. Averages were taken over locations, and azimuths, as presented in table B-2.

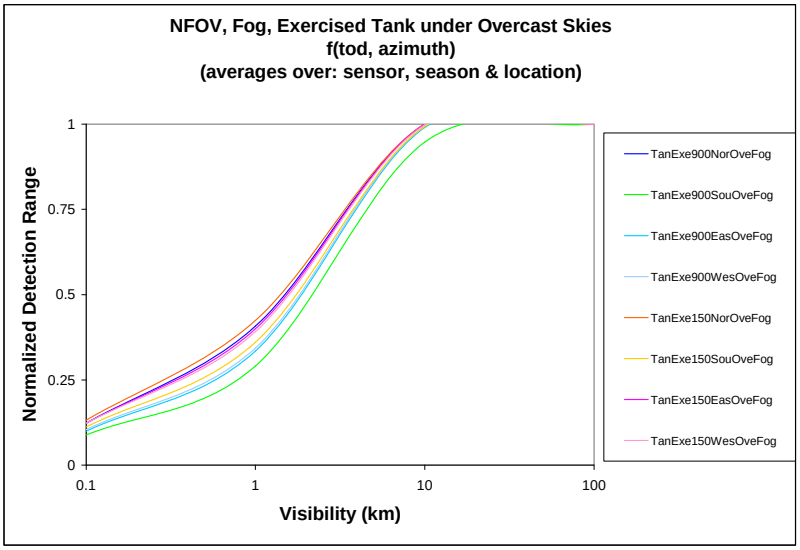


Figure B-5. Normalized detection range vs. visibility for a NFOV average sensor in a fog aerosol viewing an exercised tank under overcast skies as a function of TOD, and azimuth. Averages were taken over seasons and locations, as presented in table B-2.

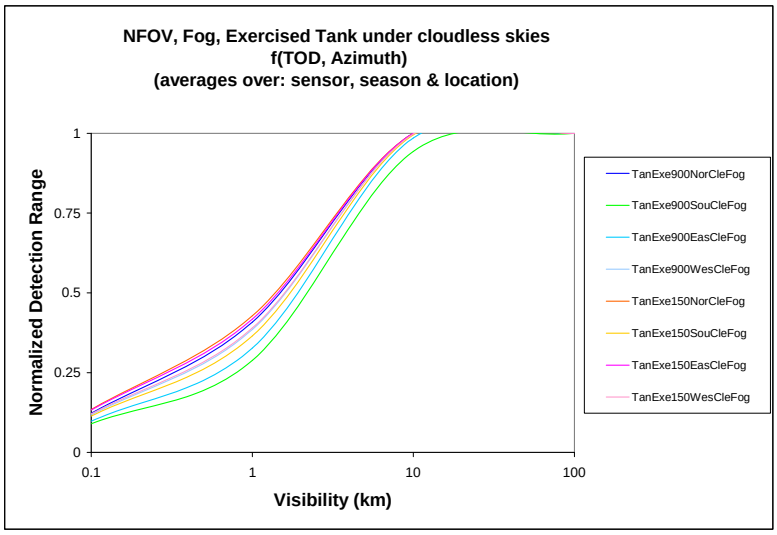


Figure B-6. Normalized detection range vs. visibility for a NFOV average sensor, in a fog aerosol, viewing an exercised tank under clear skies, as a function of TOD, and azimuth. Averages were taken over seasons and locations, as presented in table B-2.

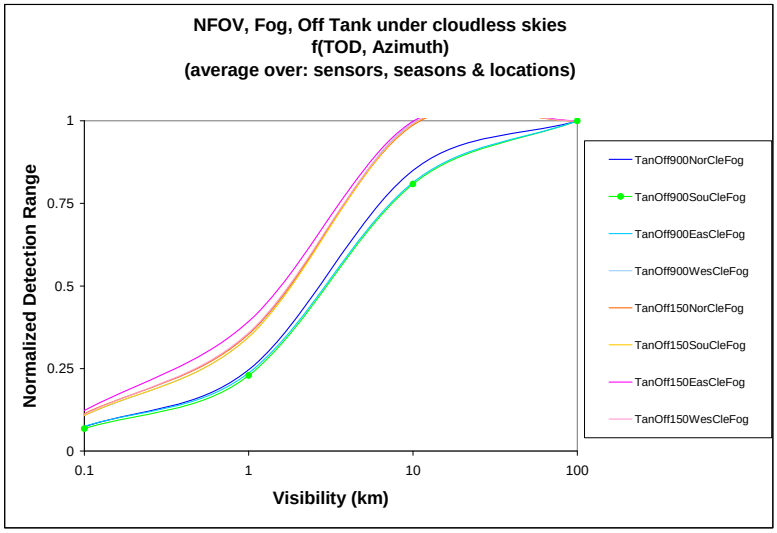


Figure B-7. Normalized detection range vs. visibility for a NFOV average sensor in a fog aerosol viewing an inactive tank under clear skies as a function of TOD, and azimuth. Averages were taken over seasons and locations, as presented in table B-2.

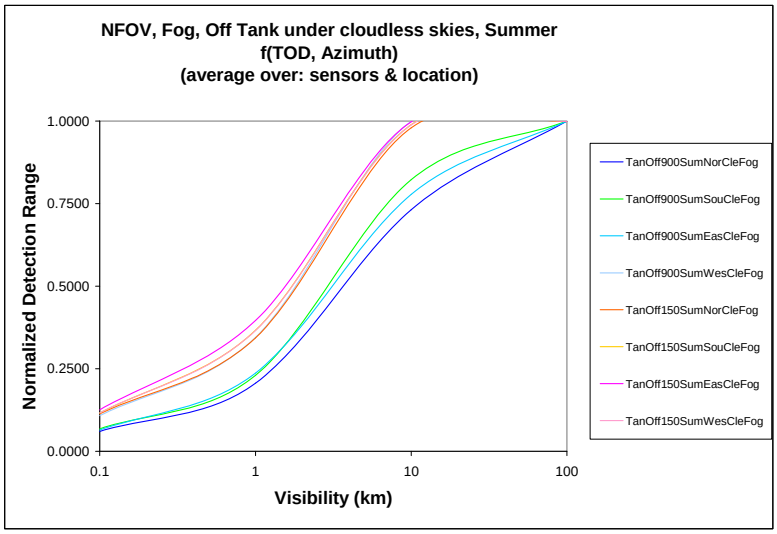


Figure B-8. Normalized detection range vs. visibility for a NFOV average sensor, in a fog aerosol, viewing an inactive tank under clear skies in the summer, as a function of TOD, and azimuth. Averages were taken over locations, as presented in table B-2.

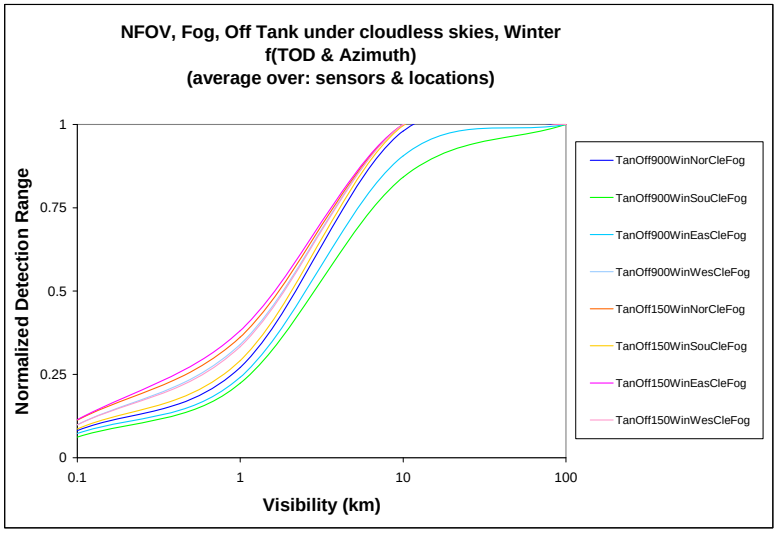


Figure B-9. Normalized detection range vs. visibility for a NFOV average sensor in a fog aerosol viewing an inactive tank under clear skies in the winter as a function of TOD, and azimuth. Averages were taken over locations, as presented in table B-2.

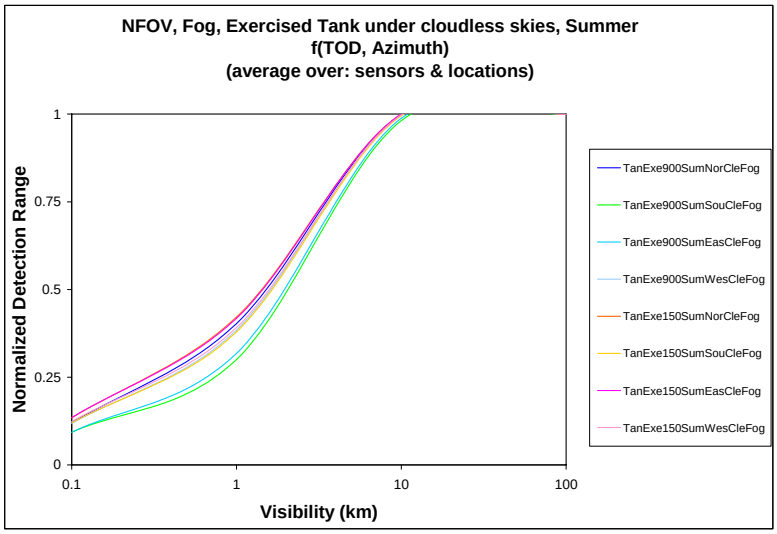


Figure B-10. Normalized detection range vs. visibility for a NFOV average sensor, in a fog aerosol, viewing an exercised tank under clear skies in the summer, as a function of TOD, and azimuth. Averages were taken over locations, as presented in table B-2.

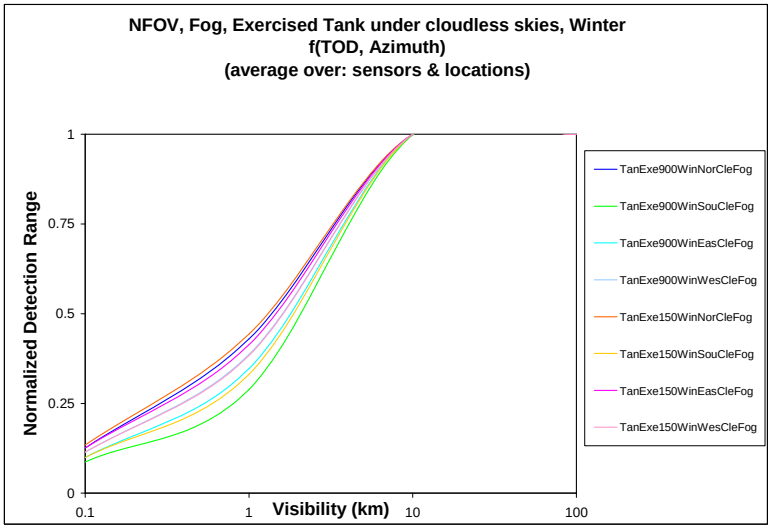


Figure B-11. Normalized detection range vs. visibility for a NFOV average sensor in a fog aerosol viewing an exercised tank under clear skies in the winter as a function of TOD, and azimuth. Averages were taken over locations, as presented in table B-2.

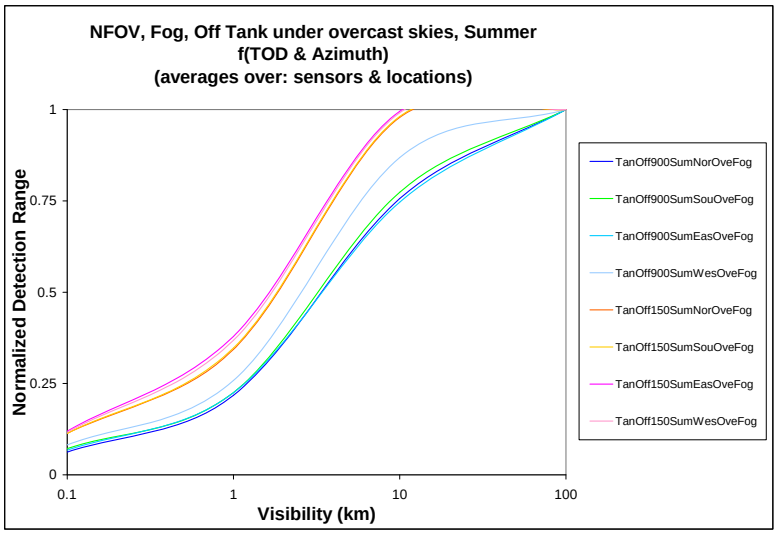


Figure B-12. Normalized detection range vs. visibility for a NFOV average sensor, in a fog aerosol, viewing an inactive tank under overcast skies in the summer, as a function of TOD, and azimuth. Averages were taken over locations, as presented in table B-2.

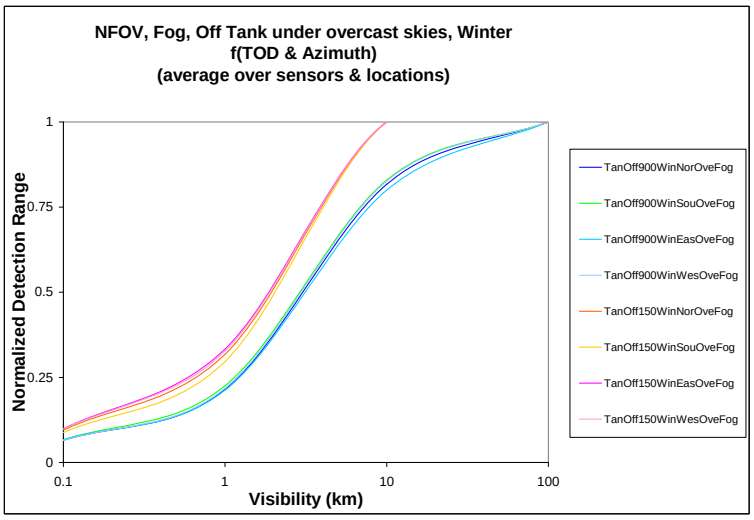


Figure B-13. Normalized detection range vs. visibility for a NFOV average sensor in a fog aerosol viewing an inactive tank under overcast skies in the winter as a function of TOD, and azimuth. Averages were taken over locations, as presented in table B-2.

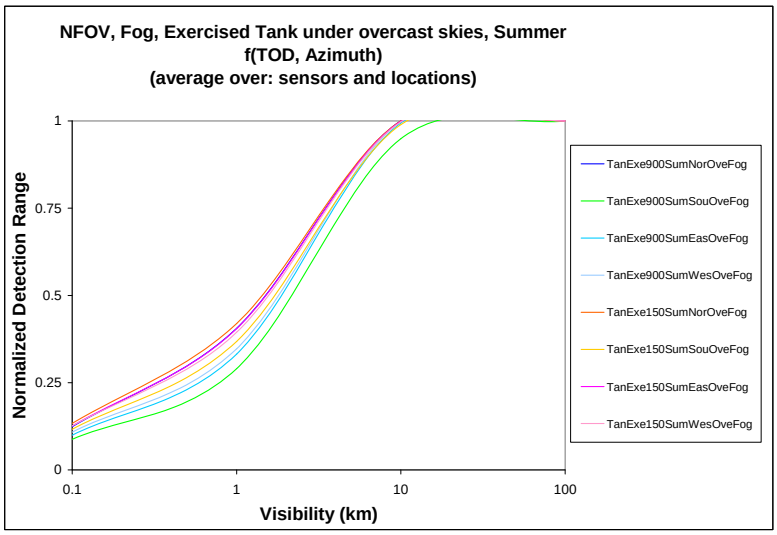


Figure B-14. Normalized detection range vs. visibility for a NFOV average sensor, in a fog aerosol, viewing an exercised tank under overcast skies in the summer, as a function of TOD, and azimuth. Averages were taken over locations, as presented in table B-2.

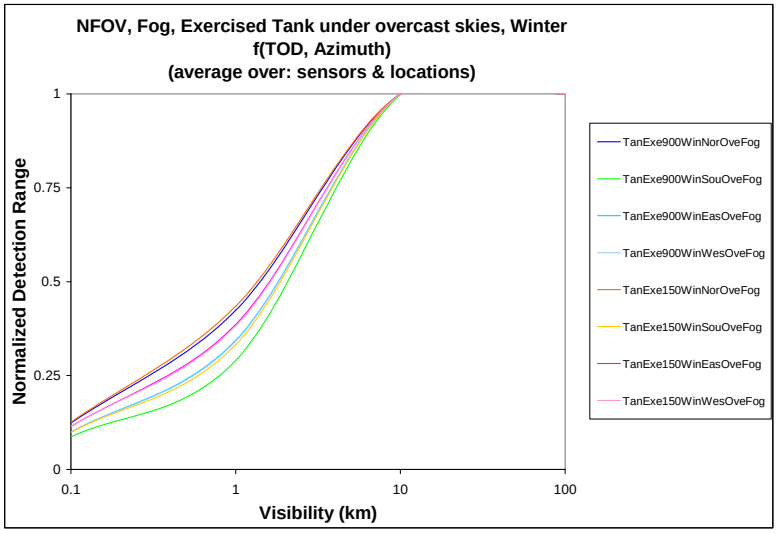


Figure B-15. Normalized detection range vs. visibility for a NFOV average sensor in a fog aerosol viewing an exercised tank under overcast skies in the winter as a function of TOD, and azimuth. Averages were taken over locations, as presented in table B-2.

# Appendix C. Third-Order Polynomial Coefficients and Their Curves for the Rural Aerosol for a NFOV and WFOV Average IR Sensor

Table C-1. Third-order polynomial coefficients curve fit to averaged quantities as represented by moniker for and average sensor viewing through a rural aerosol. WFOV results are shown.

| Moniker | a0 | a1 | a2 | a3 | Average Maximum Detection Range |
|---|---|---|---|---|---|
| 150CleRur | 0.9582 | 0.0664 | -0.0279 | 0.0034 | 3.60 |
| 150OveRur | 0.9540 | 0.0694 | -0.0284 | 0.0034 | 3.59 |
| 900CleRur | 0.8970 | 0.0915 | -0.0268 | 0.0026 | 3.48 |
| 900OveRur | 0.8346 | 0.1113 | -0.0233 | 0.0015 | 3.25 |
| Tan900CleRur | 0.9456 | 0.0678 | -0.0257 | 0.0029 | 2.73 |
| Tan150CleRur | 0.9754 | 0.0477 | -0.0219 | 0.0028 | 2.80 |
| Tan900OveRur | 0.9073 | 0.0842 | -0.0253 | 0.0025 | 2.65 |
| Tan150OveRur | 0.9747 | 0.0493 | -0.0226 | 0.0028 | 2.79 |
| TanExe150OveRur | 0.9766 | 0.0450 | -0.0206 | 0.0026 | 2.81 |
| TanExe900OveRur | 0.9708 | 0.0573 | -0.0262 | 0.0033 | 2.78 |
| TanExe150CleRur | 0.9772 | 0.0442 | -0.0203 | 0.0026 | 2.82 |
| TanExe900CleRur | 0.9720 | 0.0550 | -0.0252 | 0.0032 | 2.79 |
| TanOff900CleRur | 0.9094 | 0.0854 | -0.0263 | 0.0026 | 2.65 |
| TanOff150CleRur | 0.9736 | 0.0511 | -0.0235 | 0.0030 | 2.78 |
| TanOff150OveRur | 0.9726 | 0.0536 | -0.0247 | 0.0031 | 2.77 |
| TanOff900OveRur | 0.8421 | 0.1118 | -0.0243 | 0.0016 | 2.51 |
| TanOff900SumOveRur | 0.8262 | 0.1151 | -0.0231 | 0.0014 | 2.42 |
| TanOff900WinOveRur | 0.8216 | 0.1226 | -0.0249 | 0.0014 | 2.53 |
| TanOff150SumOveRur | 0.9732 | 0.0505 | -0.0231 | 0.0029 | 2.77 |
| TanOff150WinOveRur | 0.9703 | 0.0633 | -0.0294 | 0.0037 | 2.74 |
| TanOff900NorOveRur | 0.8016 | 0.1241 | -0.0211 | 0.0008 | 2.39 |
| TanOff900EasOveRur | 0.8195 | 0.1172 | -0.0226 | 0.0012 | 2.39 |
| TanOff900WesOveRur | 0.9143 | 0.0913 | -0.0300 | 0.0031 | 2.67 |
| TanOff900SouOveRur | 0.8290 | 0.1157 | -0.0231 | 0.0013 | 2.58 |
| TanExe900SumOveRur | 0.9702 | 0.0575 | -0.0263 | 0.0033 | 2.78 |
| TanExe900WinOveRur | 0.9731 | 0.0578 | -0.0271 | 0.0034 | 2.79 |
| TanExe150SumOveRur | 0.9764 | 0.0437 | -0.0198 | 0.0025 | 2.81 |
| TanExe150WinOveRur | 0.9773 | 0.0487 | -0.0229 | 0.0029 | 2.81 |
| TanExe900NorOveRur | 0.9787 | 0.0429 | -0.0197 | 0.0025 | 2.85 |
| TanExe900EasOveRur | 0.9713 | 0.0583 | -0.0271 | 0.0034 | 2.77 |
| TanExe900WesOveRur | 0.9717 | 0.0571 | -0.0264 | 0.0033 | 2.78 |
| TanExe900SouOveRur | 0.9610 | 0.0709 | -0.0315 | 0.0039 | 2.73 |
| TanExe150NorOveRur | 0.9792 | 0.0405 | -0.0184 | 0.0023 | 2.85 |
| TanExe150EasOveRur | 0.9771 | 0.0433 | -0.0198 | 0.0025 | 2.82 |
| TanExe150WesOveRur | 0.9766 | 0.0447 | -0.0205 | 0.0026 | 2.81 |

Table C-1. Third-order polynomial coefficients curve fit to averaged quantities as represented by moniker for and average sensor viewing through a rural aerosol. WFOV results are shown (continued).

| Moniker | a0 | a1 | a2 | a3 | Average Maximum Detection Range |
|---|---|---|---|---|---|
| TanExe150SouOveRur | 0.9736 | 0.0514 | -0.0236 | 0.0030 | 2.78 |
| TanExe900NorCleRur | 0.9790 | 0.0424 | -0.0195 | 0.0024 | 2.85 |
| TanExe900EasCleRur | 0.9711 | 0.0597 | -0.0278 | 0.0035 | 2.76 |
| TanExe900WesCleRur | 0.9762 | 0.0469 | -0.0215 | 0.0027 | 2.82 |
| TanExe900SouCleRur | 0.9612 | 0.0712 | -0.0317 | 0.0039 | 2.72 |
| TanExe150NorCleRur | 0.9799 | 0.0397 | -0.0181 | 0.0023 | 2.85 |
| TanExe150EasCleRur | 0.9781 | 0.0416 | -0.0189 | 0.0024 | 2.83 |
| TanExe150WesCleRur | 0.9768 | 0.0453 | -0.0210 | 0.0027 | 2.80 |
| TanExe150SouCleRur | 0.9740 | 0.0503 | -0.0231 | 0.0029 | 2.79 |
| TanOff900NorCleRur | 0.8869 | 0.0970 | -0.0263 | 0.0023 | 2.69 |
| TanOff900EasCleRur | 0.8805 | 0.0988 | -0.0263 | 0.0023 | 2.61 |
| TanOff900WesCleRur | 0.9715 | 0.0555 | -0.0253 | 0.0032 | 2.79 |
| TanOff900SouCleRur | 0.8682 | 0.1051 | -0.0274 | 0.0023 | 2.49 |
| TanOff150NorCleRur | 0.9729 | 0.0520 | -0.0239 | 0.0030 | 2.78 |
| TanOff150EasCleRur | 0.9764 | 0.0450 | -0.0205 | 0.0026 | 2.81 |
| TanOff150WesCleRur | 0.9733 | 0.0525 | -0.0243 | 0.0031 | 2.77 |
| TanOff150SouCleRur | 0.9717 | 0.0549 | -0.0253 | 0.0032 | 2.77 |
| TanOff900SumNorCleRur | 0.7072 | 0.1484 | -0.0085 | -0.0022 | 2.62 |
| TanOff900SumEasCleRur | 0.7828 | 0.1273 | -0.0180 | 0.0001 | 2.84 |
| TanOff900SumWesCleRur | 0.9716 | 0.0560 | -0.0254 | 0.0032 | 2.78 |
| TanOff900SumSouCleRur | 0.8965 | 0.0971 | -0.0287 | 0.0027 | 2.71 |
| TanOff150SumNorCleRur | 0.9723 | 0.0531 | -0.0245 | 0.0031 | 2.76 |
| TanOff150SumEasCleRur | 0.9763 | 0.0442 | -0.0200 | 0.0025 | 2.81 |
| TanOff150SumWesCleRur | 0.9739 | 0.0502 | -0.0232 | 0.0029 | 2.78 |
| TanOff150SumSouCleRur | 0.9740 | 0.0489 | -0.0222 | 0.0028 | 2.78 |
| TanOff900WinNorCleRur | 0.9574 | 0.0772 | -0.0341 | 0.0042 | 2.74 |
| TanOff90Win0EasCleRur | 0.9161 | 0.0918 | -0.0312 | 0.0033 | 2.70 |
| TanOff900WinWesCleRur | 0.9706 | 0.0589 | -0.0271 | 0.0034 | 2.80 |
| TanOff900WinSouCleRur | 0.8650 | 0.1096 | -0.0306 | 0.0029 | 2.44 |
| TanOff150WinNorCleRur | 0.9735 | 0.0516 | -0.0236 | 0.0030 | 2.83 |
| TanOff150WinEasCleRur | 0.9764 | 0.0480 | -0.0223 | 0.0028 | 2.81 |
| TanOff150WinWesCleRur | 0.9714 | 0.0604 | -0.0280 | 0.0035 | 2.76 |
| TanOff150WinSouCleRur | 0.9649 | 0.0705 | -0.0326 | 0.0041 | 2.74 |
| TanExe900SumNorCleRur | 0.9782 | 0.0434 | -0.0199 | 0.0025 | 2.85 |
| TanExe900SumEasCleRur | 0.9695 | 0.0616 | -0.0287 | 0.0036 | 2.75 |
| TanExe900SumWesCleRur | 0.9762 | 0.0468 | -0.0215 | 0.0027 | 2.81 |
| TanExe900SumSouCleRur | 0.9671 | 0.0658 | -0.0302 | 0.0038 | 2.74 |
| TanExe150SumNorCleRur | 0.9778 | 0.0410 | -0.0183 | 0.0023 | 2.85 |
| TanExe150SumEasCleRur | 0.9772 | 0.0413 | -0.0186 | 0.0023 | 2.83 |
| TanExe150SumWesCleRur | 0.9764 | 0.0446 | -0.0206 | 0.0026 | 2.80 |
| TanExe150SumSouCleRur | 0.9747 | 0.0464 | -0.0211 | 0.0027 | 2.81 |
| TanExe900WinNorCleRur | 0.9837 | 0.0395 | -0.0191 | 0.0025 | 2.85 |
| TanExe90Win0EasCleRur | 0.9741 | 0.0566 | -0.0265 | 0.0033 | 2.78 |
| TanExe900WinWesCleRur | 0.9764 | 0.0477 | -0.0223 | 0.0028 | 2.85 |

Table C-1. Third-order polynomial coefficients curve fit to averaged quantities as represented by moniker for and average sensor viewing through a rural aerosol. WFOV results are shown (continued).

| Moniker | a0 | a1 | a2 | a3 | Average Maximum Detection Range |
|---|---|---|---|---|---|
| TanExe900WinSouCleRur | 0.9645 | 0.0736 | -0.0340 | 0.0043 | 2.74 |
| TanExe150WinNorCleRur | 0.9852 | 0.0370 | -0.0180 | 0.0023 | 2.85 |
| TanExe150WinEasCleRur | 0.9796 | 0.0427 | -0.0199 | 0.0025 | 2.85 |
| TanExe150WinWesCleRur | 0.9774 | 0.0483 | -0.0228 | 0.0029 | 2.81 |
| TanExe150WinSouCleRur | 0.9721 | 0.0603 | -0.0281 | 0.0035 | 2.76 |
| TanOff900SumNorOveRur | 0.7385 | 0.1382 | -0.0148 | -0.0006 | 2.20 |
| TanOff900SumEasOveRur | 0.7629 | 0.1332 | -0.0180 | 0.0001 | 2.10 |
| TanOff900SumWesOveRur | 0.9414 | 0.0825 | -0.0323 | 0.0037 | 2.68 |
| TanOff900SumSouOveRur | 0.8291 | 0.1148 | -0.0243 | 0.0016 | 2.62 |
| TanOff150SumNorOveRur | 0.9717 | 0.0543 | -0.0250 | 0.0032 | 2.75 |
| TanOff150SumEasOveRur | 0.9750 | 0.0467 | -0.0212 | 0.0026 | 2.79 |
| TanOff150SumWesOveRur | 0.9739 | 0.0486 | -0.0222 | 0.0028 | 2.78 |
| TanOff150SumSouOveRur | 0.9720 | 0.0526 | -0.0241 | 0.0030 | 2.77 |
| TanOff900WinNorOveRur | 0.8006 | 0.1269 | -0.0239 | 0.0013 | 2.47 |
| TanOff900Win0EasOveRu | 0.8508 | 0.1136 | -0.0279 | 0.0022 | 2.56 |
| TanOff900WinWesOveRur | 0.8532 | 0.1159 | -0.0270 | 0.0019 | 2.63 |
| TanOff900WinSouOveRur | 0.7820 | 0.1339 | -0.0205 | 0.0004 | 2.45 |
| TanOff150WinNorOveRur | 0.9701 | 0.0626 | -0.0289 | 0.0036 | 2.74 |
| TanOff150WinEasOveRur | 0.9727 | 0.0599 | -0.0281 | 0.0035 | 2.74 |
| TanOff150WinWesOveRur | 0.9715 | 0.0611 | -0.0284 | 0.0036 | 2.74 |
| TanOff150WinSouOveRur | 0.9667 | 0.0698 | -0.0321 | 0.0040 | 2.73 |
| TanExe900SumNorOveRur | 0.9782 | 0.0434 | -0.0199 | 0.0025 | 2.85 |
| TanExe900SumEasOveRur | 0.9697 | 0.0603 | -0.0280 | 0.0035 | 2.77 |
| TanExe900SumWesOveRur | 0.9723 | 0.0554 | -0.0255 | 0.0032 | 2.78 |
| TanExe900SumSouOveRur | 0.9600 | 0.0713 | -0.0317 | 0.0039 | 2.72 |
| TanExe150SumNorOveRur | 0.9777 | 0.0412 | -0.0184 | 0.0023 | 2.85 |
| TanExe150SumEasOveRur | 0.9774 | 0.0414 | -0.0187 | 0.0023 | 2.81 |
| TanExe150SumWesOveRur | 0.9764 | 0.0434 | -0.0198 | 0.0025 | 2.81 |
| TanExe150SumSouOveRur | 0.9739 | 0.0486 | -0.0222 | 0.0028 | 2.78 |
| TanExe900WinNorOveRur | 0.9828 | 0.0403 | -0.0193 | 0.0025 | 2.85 |
| TanExe900WinEasOveRur | 0.9727 | 0.0578 | -0.0271 | 0.0034 | 2.78 |
| TanExe900WinWesOveRur | 0.9717 | 0.0604 | -0.0283 | 0.0036 | 2.78 |
| TanExe900WinSouOveRur | 0.9644 | 0.0728 | -0.0335 | 0.0042 | 2.75 |
| TanExe150WinNorOveRur | 0.9832 | 0.0393 | -0.0188 | 0.0024 | 2.85 |
| TanExe150WinEasOveRur | 0.9772 | 0.0475 | -0.0222 | 0.0028 | 2.81 |
| TanExe150WinWesOveRur | 0.9769 | 0.0484 | -0.0227 | 0.0029 | 2.81 |
| TanExe150WinSouOveRur | 0.9718 | 0.0597 | -0.0277 | 0.0035 | 2.77 |

Table C-2. Third-order polynomial coefficients curve fit to averaged quantities as represented by moniker for an average sensor viewing through a rural aerosol. NFOV results are shown. Coefficients in blue have associated curves presented in the graphs in this appendix.

| Moniker | a0 | a1 | a2 | a3 | Average Maximum Detection Range |
|---|---|---|---|---|---|
| 150CleRur | 0.8336 | 0.1492 | -0.0400 | 0.0033 | 8.88 |
| 150OveRur | 0.8187 | 0.1529 | -0.0378 | 0.0029 | 8.88 |
| 900CleRur | 0.7362 | 0.1679 | -0.0276 | 0.0008 | 8.65 |
| 900OveRur | 0.6396 | 0.1812 | -0.0143 | -0.0018 | 8.12 |
| Tan900CleRur | 0.8115 | 0.1505 | -0.0369 | 0.0028 | 7.67 |
| Tan150CleRur | 0.8913 | 0.1320 | -0.0462 | 0.0049 | 7.80 |
| Tan900OveRur | 0.7347 | 0.1652 | -0.0264 | 0.0007 | 7.50 |
| Tan150OveRur | 0.8832 | 0.1345 | -0.0453 | 0.0047 | 7.80 |
| TanExe150OveRur | 0.9061 | 0.1280 | -0.0481 | 0.0054 | 7.80 |
| TanExe900OveRur | 0.8552 | 0.1434 | -0.0425 | 0.0039 | 7.80 |
| TanExe150CleRur | 0.9103 | 0.1264 | -0.0484 | 0.0055 | 7.80 |
| TanExe900CleRur | 0.8657 | 0.1399 | -0.0436 | 0.0043 | 7.80 |
| TanOff900CleRur | 0.7399 | 0.1643 | -0.0280 | 0.0010 | 7.49 |
| TanOff150CleRur | 0.8723 | 0.1376 | -0.0440 | 0.0044 | 7.80 |
| TanOff150OveRur | 0.8604 | 0.1409 | -0.0426 | 0.0040 | 7.80 |
| TanOff900OveRur | 0.6085 | 0.1864 | -0.0099 | -0.0026 | 7.18 |
| TanOff900SumOveRur | 0.5971 | 0.1860 | -0.0091 | -0.0027 | 6.98 |
| TanOff900WinOveRur | 0.5940 | 0.1951 | -0.0080 | -0.0033 | 7.57 |
| TanOff150SumOveRur | 0.8554 | 0.1405 | -0.0410 | 0.0037 | 7.80 |
| TanOff150WinOveRur | 0.8677 | 0.1439 | -0.0462 | 0.0046 | 7.80 |
| TanOff900NorOveRur | 0.5746 | 0.1902 | -0.0058 | -0.0034 | 6.91 |
| TanOff900EasOveRur | 0.5900 | 0.1833 | -0.0085 | -0.0026 | 6.63 |
| TanOff900WesOveRur | 0.6787 | 0.1816 | -0.0180 | -0.0014 | 7.78 |
| TanOff900SouOveRur | 0.5854 | 0.1907 | -0.0069 | -0.0033 | 7.36 |
| TanExe900SumOveRur | 0.8563 | 0.1431 | -0.0426 | 0.0040 | 7.80 |
| TanExe900WinOveRur | 0.8926 | 0.1371 | -0.0493 | 0.0053 | 7.80 |
| TanExe150SumOveRur | 0.8961 | 0.1295 | -0.0461 | 0.0050 | 7.80 |
| TanExe150WinOveRur | 0.9318 | 0.1248 | -0.0535 | 0.0064 | 7.80 |
| TanExe900NorOveRur | 0.9308 | 0.1224 | -0.0519 | 0.0062 | 7.80 |
| TanExe900EasOveRur | 0.8494 | 0.1457 | -0.0422 | 0.0038 | 7.80 |
| TanExe900WesOveRur | 0.8663 | 0.1412 | -0.0444 | 0.0043 | 7.80 |
| TanExe900SouOveRur | 0.7741 | 0.1638 | -0.0315 | 0.0014 | 7.80 |
| TanExe150NorOveRur | 0.9269 | 0.1207 | -0.0499 | 0.0059 | 7.80 |
| TanExe150EasOveRur | 0.9138 | 0.1259 | -0.0491 | 0.0056 | 7.80 |
| TanExe150WesOveRur | 0.9068 | 0.1279 | -0.0482 | 0.0054 | 7.80 |
| TanExe150SouOveRur | 0.8770 | 0.1374 | -0.0452 | 0.0046 | 7.80 |
| TanExe900NorCleRur | 0.9315 | 0.1221 | -0.0519 | 0.0062 | 7.80 |
| TanExe900EasCleRur | 0.8406 | 0.1475 | -0.0407 | 0.0035 | 7.80 |
| TanExe900WesCleRur | 0.9186 | 0.1264 | -0.0507 | 0.0059 | 7.80 |
| TanExe900SouCleRur | 0.7718 | 0.1632 | -0.0313 | 0.0014 | 7.80 |
| TanExe150NorCleRur | 0.9282 | 0.1202 | -0.0500 | 0.0059 | 7.80 |
| TanExe150EasCleRur | 0.9241 | 0.1216 | -0.0496 | 0.0058 | 7.80 |
| TanExe150WesCleRur | 0.9051 | 0.1283 | -0.0480 | 0.0053 | 7.80 |

Table C-2. Third-order polynomial coefficients curve fit to averaged quantities as represented by moniker for an average sensor viewing through a rural aerosol. NFOV results are shown. Coefficients in blue have associated curves presented in the graphs in this appendix (continued).

| Moniker | a0 | a1 | a2 | a3 | Average Maximum Detection Range |
|---|---|---|---|---|---|
| TanExe150SouCleRur | 0.8839 | 0.1354 | -0.0460 | 0.0048 | 7.80 |
| TanOff900NorCleRur | 0.6740 | 0.1789 | -0.0186 | -0.0011 | 7.84 |
| TanOff900EasCleRur | 0.7214 | 0.1681 | -0.0258 | 0.0005 | 7.19 |
| TanOff900WesCleRur | 0.8778 | 0.1388 | -0.0462 | 0.0047 | 7.80 |
| TanOff900SouCleRur | 0.6381 | 0.1795 | -0.0154 | -0.0014 | 7.03 |
| TanOff150NorCleRur | 0.8639 | 0.1399 | -0.0430 | 0.0041 | 7.80 |
| TanOff150EasCleRur | 0.9089 | 0.1273 | -0.0485 | 0.0055 | 7.80 |
| TanOff150WesCleRur | 0.8697 | 0.1387 | -0.0439 | 0.0043 | 7.80 |
| TanOff150SouCleRur | 0.8467 | 0.1443 | -0.0407 | 0.0036 | 7.80 |
| TanOff900SumNorCleRur | 0.4846 | 0.2042 | 0.0064 | -0.0057 | 8.05 |
| TanOff900SumEasCleRur | 0.5682 | 0.2018 | -0.0033 | -0.0044 | 8.34 |
| TanOff900SumWesCleRur | 0.8754 | 0.1394 | -0.0459 | 0.0047 | 7.80 |
| TanOff900SumSouCleRur | 0.6589 | 0.1820 | -0.0164 | -0.0015 | 7.74 |
| TanOff150SumNorCleRur | 0.8315 | 0.1464 | -0.0376 | 0.0030 | 7.80 |
| TanOff150SumEasCleRur | 0.8986 | 0.1284 | -0.0463 | 0.0050 | 7.80 |
| TanOff150SumWesCleRur | 0.8620 | 0.1390 | -0.0419 | 0.0040 | 7.80 |
| TanOff150SumSouCleRur | 0.8655 | 0.1384 | -0.0426 | 0.0041 | 7.80 |
| TanOff900WinNorCleRur | 0.7827 | 0.1641 | -0.0340 | 0.0019 | 7.80 |
| TanOff90Win0EasCleRur | 0.7223 | 0.1775 | -0.0251 | -0.0001 | 7.80 |
| TanOff900WinWesCleRur | 0.9160 | 0.1335 | -0.0539 | 0.0063 | 7.80 |
| TanOff900WinSouCleRur | 0.6477 | 0.1778 | -0.0185 | -0.0008 | 6.87 |
| TanOff150WinNorCleRur | 0.9293 | 0.1277 | -0.0544 | 0.0065 | 7.80 |
| TanOff150WinEasCleRur | 0.9381 | 0.1242 | -0.0549 | 0.0067 | 7.80 |
| TanOff150WinWesCleRur | 0.8928 | 0.1378 | -0.0498 | 0.0054 | 7.80 |
| TanOff150WinSouCleRur | 0.8095 | 0.1579 | -0.0378 | 0.0027 | 7.80 |
| TanExe900SumNorCleRur | 0.9349 | 0.1223 | -0.0530 | 0.0064 | 7.80 |
| TanExe900SumEasCleRur | 0.8188 | 0.1525 | -0.0375 | 0.0028 | 7.80 |
| TanExe900SumWesCleRur | 0.9208 | 0.1260 | -0.0511 | 0.0060 | 7.80 |
| TanExe900SumSouCleRur | 0.8008 | 0.1573 | -0.0352 | 0.0023 | 7.80 |
| TanExe150SumNorCleRur | 0.9190 | 0.1224 | -0.0486 | 0.0056 | 7.80 |
| TanExe150SumEasCleRur | 0.9143 | 0.1231 | -0.0477 | 0.0054 | 7.80 |
| TanExe150SumWesCleRur | 0.8938 | 0.1301 | -0.0459 | 0.0049 | 7.80 |
| TanExe150SumSouCleRur | 0.8852 | 0.1332 | -0.0452 | 0.0047 | 7.80 |
| TanExe900WinNorCleRur | 0.9523 | 0.1160 | -0.0544 | 0.0068 | 7.80 |
| TanExe90Win0EasCleRur | 0.9215 | 0.1307 | -0.0539 | 0.0063 | 7.80 |
| TanExe900WinWesCleRur | 0.9437 | 0.1220 | -0.0553 | 0.0068 | 7.80 |
| TanExe900WinSouCleRur | 0.8124 | 0.1580 | -0.0387 | 0.0029 | 7.80 |
| TanExe150WinNorCleRur | 0.9531 | 0.1147 | -0.0539 | 0.0068 | 7.80 |
| TanExe150WinEasCleRur | 0.9487 | 0.1185 | -0.0548 | 0.0068 | 7.80 |
| TanExe150WinWesCleRur | 0.9389 | 0.1229 | -0.0544 | 0.0066 | 7.80 |
| TanExe150WinSouCleRur | 0.8895 | 0.1391 | -0.0496 | 0.0053 | 7.80 |
| TanOff900SumNorOveRur | 0.5360 | 0.1896 | -0.0022 | -0.0037 | 6.87 |
| TanOff900SumEasOveRur | 0.5363 | 0.1841 | -0.0027 | -0.0034 | 5.73 |
| TanOff900SumWesOveRur | 0.7051 | 0.1792 | -0.0215 | -0.0008 | 7.80 |

Table C-2. Third-order polynomial coefficients curve fit to averaged quantities as represented by moniker for an average sensor viewing through a rural aerosol. NFOV results are shown. Coefficients in blue have associated curves presented in the graphs in this appendix (continued).

| Moniker | a0 | a1 | a2 | a3 | Average Maximum Detection Range |
|---|---|---|---|---|---|
| TanOff900SumSouOveRur | 0.5804 | 0.1914 | -0.0068 | -0.0032 | 7.38 |
| TanOff150SumNorOveRur | 0.8304 | 0.1466 | -0.0375 | 0.0030 | 7.80 |
| TanOff150SumEasOveRur | 0.8864 | 0.1325 | -0.0451 | 0.0047 | 7.80 |
| TanOff150SumWesOveRur | 0.8664 | 0.1380 | -0.0426 | 0.0041 | 7.80 |
| TanOff150SumSouOveRur | 0.8385 | 0.1447 | -0.0386 | 0.0032 | 7.80 |
| TanOff900WinNorOveRur | 0.5750 | 0.2012 | -0.0044 | -0.0042 | 7.53 |
| TanOff900Win0EasOveRu | 0.6146 | 0.1897 | -0.0114 | -0.0025 | 7.52 |
| TanOff900WinWesOveRur | 0.6301 | 0.1856 | -0.0134 | -0.0021 | 7.72 |
| TanOff900WinSouOveRur | 0.5527 | 0.2039 | -0.0024 | -0.0045 | 7.49 |
| TanOff150WinNorOveRur | 0.8636 | 0.1447 | -0.0455 | 0.0044 | 7.80 |
| TanOff150WinEasOveRur | 0.8982 | 0.1365 | -0.0506 | 0.0056 | 7.80 |
| TanOff150WinWesOveRur | 0.8884 | 0.1388 | -0.0491 | 0.0053 | 7.80 |
| TanOff150WinSouOveRur | 0.8206 | 0.1556 | -0.0396 | 0.0031 | 7.80 |
| TanExe900SumNorOveRur | 0.9352 | 0.1217 | -0.0528 | 0.0064 | 7.80 |
| TanExe900SumEasOveRur | 0.8419 | 0.1475 | -0.0411 | 0.0036 | 7.80 |
| TanExe900SumWesOveRur | 0.8765 | 0.1387 | -0.0458 | 0.0047 | 7.80 |
| TanExe900SumSouOveRur | 0.7716 | 0.1641 | -0.0310 | 0.0013 | 7.80 |
| TanExe150SumNorOveRur | 0.9173 | 0.1229 | -0.0484 | 0.0056 | 7.80 |
| TanExe150SumEasOveRur | 0.9054 | 0.1269 | -0.0473 | 0.0053 | 7.80 |
| TanExe150SumWesOveRur | 0.8961 | 0.1297 | -0.0463 | 0.0050 | 7.80 |
| TanExe150SumSouOveRur | 0.8655 | 0.1384 | -0.0426 | 0.0041 | 7.80 |
| TanExe900WinNorOveRur | 0.9510 | 0.1171 | -0.0546 | 0.0068 | 7.80 |
| TanExe900WinEasOveRur | 0.9065 | 0.1360 | -0.0526 | 0.0060 | 7.80 |
| TanExe900WinWesOveRur | 0.8995 | 0.1372 | -0.0513 | 0.0057 | 7.80 |
| TanExe900WinSouOveRur | 0.8134 | 0.1579 | -0.0389 | 0.0029 | 7.80 |
| TanExe150WinNorOveRur | 0.9517 | 0.1158 | -0.0541 | 0.0068 | 7.80 |
| TanExe150WinEasOveRur | 0.9398 | 0.1225 | -0.0545 | 0.0067 | 7.80 |
| TanExe150WinWesOveRur | 0.9369 | 0.1237 | -0.0543 | 0.0066 | 7.80 |
| TanExe150WinSouOveRur | 0.8986 | 0.1370 | -0.0510 | 0.0056 | 7.80 |

The coefficients displayed in blue in table C-2 have associated curves that are presented in the following graphs labeled figures C-1 through C-15.

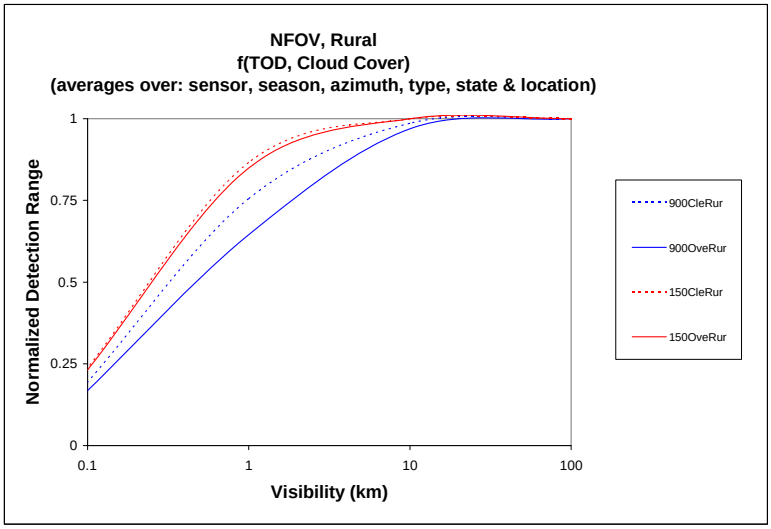


Figure C-1. Normalized detection range vs. visibility for a NFOV average sensor in a rural aerosol as a function of TOD, and cloud cover. Averages were taken over seasons, locations, azimuths, target types and operating states, as presented in table C-2.

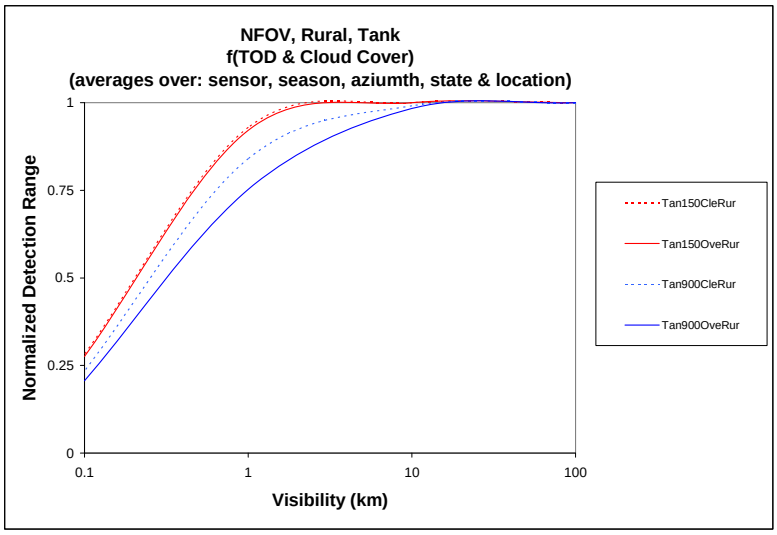


Figure C-2. Normalized detection range vs. visibility for a NFOV average sensor, in a rural aerosol, viewing a tank, as a function of TOD, and cloud cover. Averages were taken over seasons, locations, azimuths, and target operating states, as presented in table C-2.

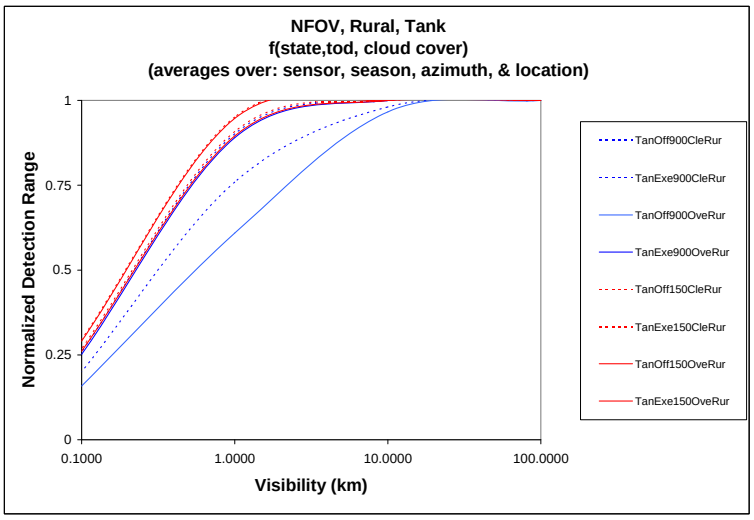


Figure C-3. Normalized detection range vs. visibility for a NFOV average sensor in a rural aerosol as a function of target operating state, TOD, and cloud cover. Averages were taken over seasons, locations, and azimuths, as presented in table C-2.

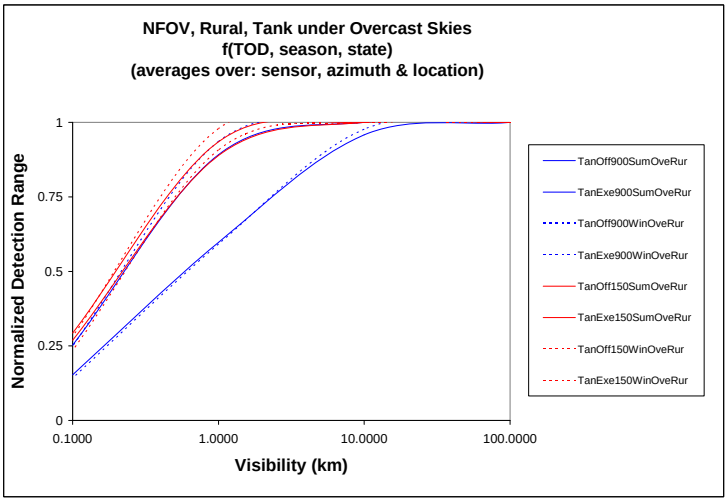


Figure C-4. Normalized detection range vs. visibility for a NFOV average sensor, in a rural aerosol, viewing a tank under overcast skies, as a function of TOD, season, and operating state. Averages were taken over locations, and azimuths, as presented in table C-2.

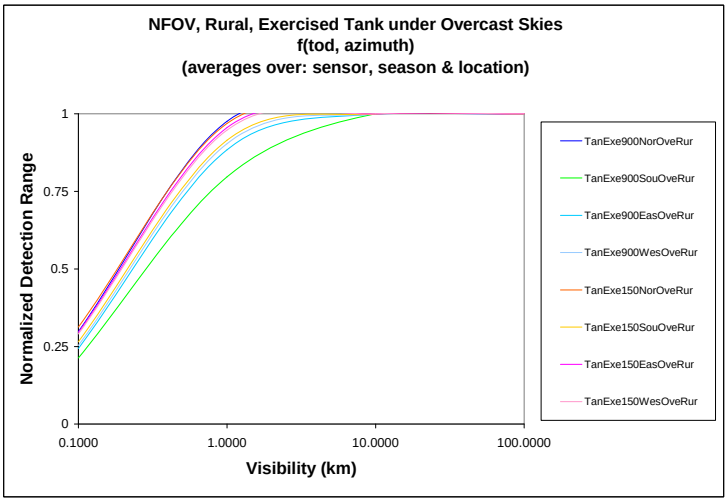


Figure C-5. Normalized detection range vs. visibility for a NFOV average sensor in a rural aerosol viewing an exercised tank under overcast skies as a function of TOD, and azimuth. Averages were taken over seasons and locations, as presented in table C-2.

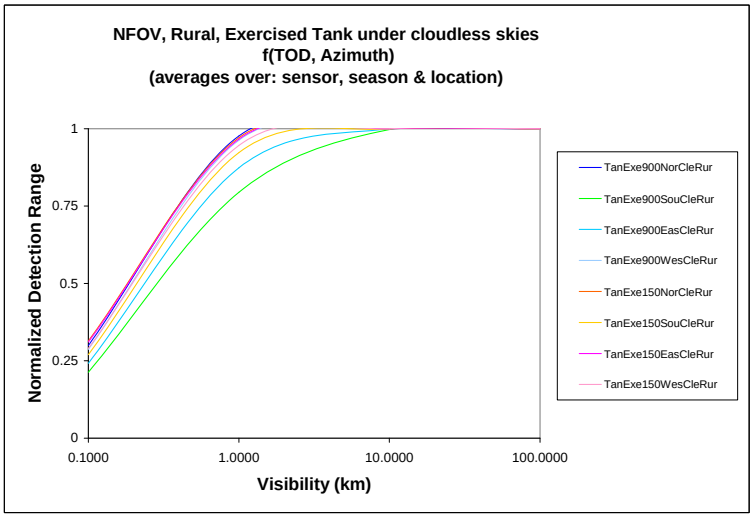


Figure C-6. Normalized detection range vs. visibility for a NFOV average sensor, in a rural aerosol, viewing an exercised tank under clear skies, as a function of TOD, and azimuth. Averages were taken over seasons and locations, as presented in table C-2.

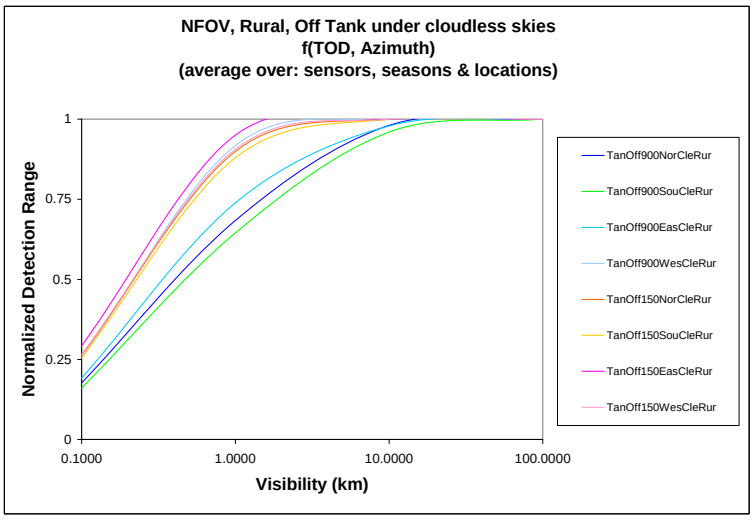


Figure C-7. Normalized detection range vs. visibility for a NFOV average sensor in a rural aerosol viewing an inactive tank under clear skies as a function of TOD, and azimuth. Averages were taken over seasons and locations, as presented in table C-2.

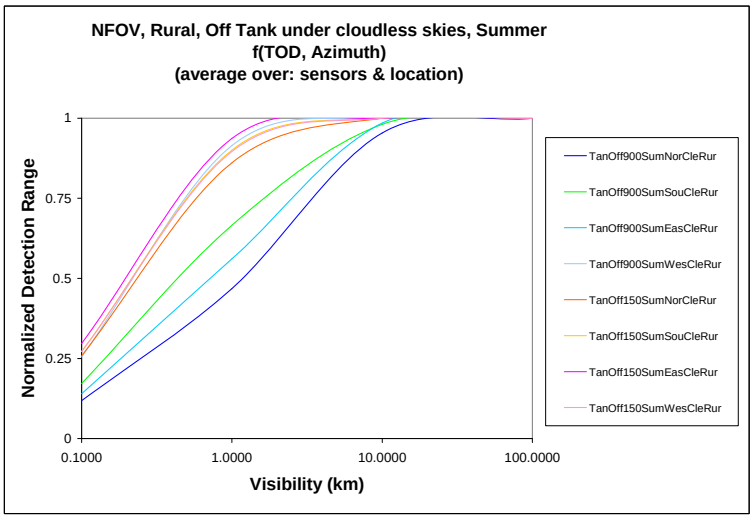


Figure C-8. Normalized detection range vs. visibility for a NFOV average sensor, in a rural aerosol, viewing an inactive tank under clear skies in the summer, as a function of TOD, and azimuth. Averages were taken over locations, as presented in table C-2.

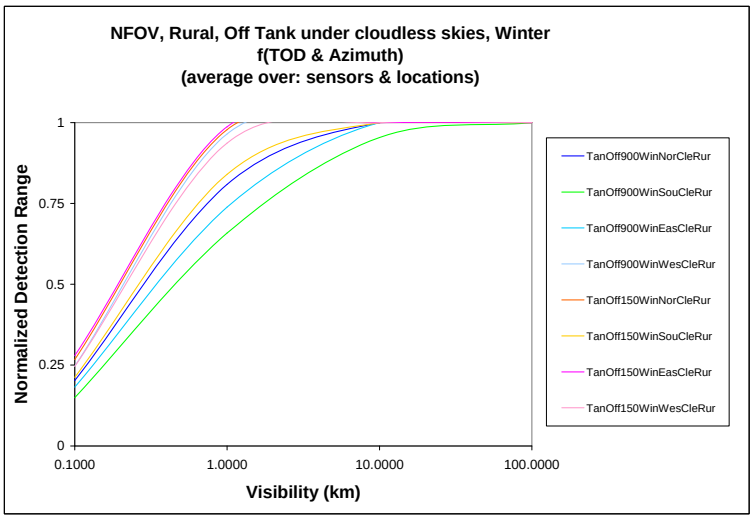


Figure C-9. Normalized detection range vs. visibility for a NFOV average sensor in a rural aerosol viewing an inactive tank under clear skies in the winter as a function of TOD, and azimuth. Averages were taken over locations, as presented in table C-2.

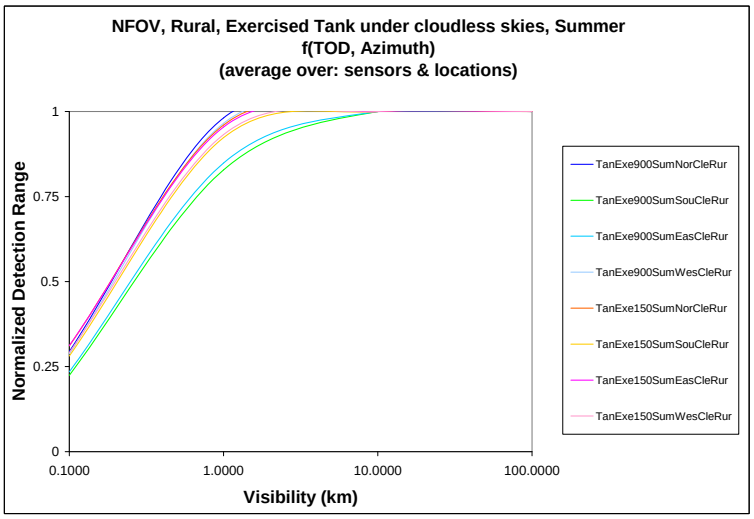


Figure C-10. Normalized detection range vs. visibility for a NFOV average sensor, in a rural aerosol, viewing an exercised tank under clear skies in the summer, as a function of TOD, and azimuth. Averages were taken over locations, as presented in table C-2.

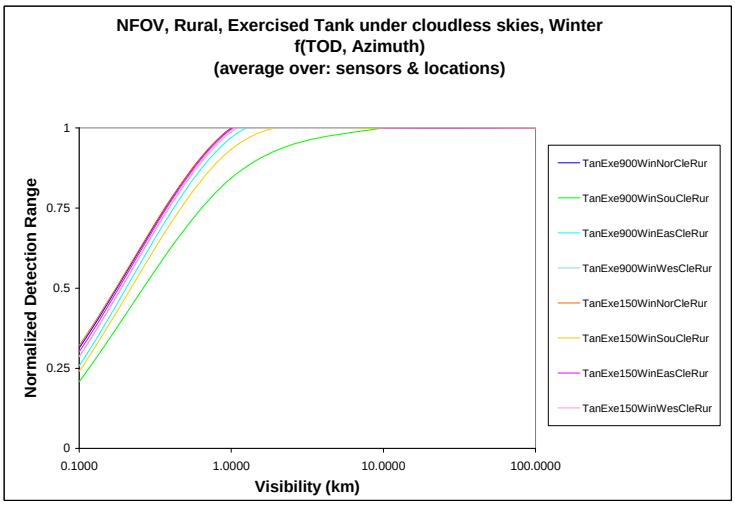


Figure C-11. Normalized detection range vs. visibility for a NFOV average sensor in a rural aerosol viewing an exercised tank under clear skies in the winter as a function of TOD, and azimuth. Averages were taken over locations, as presented in table c-2.

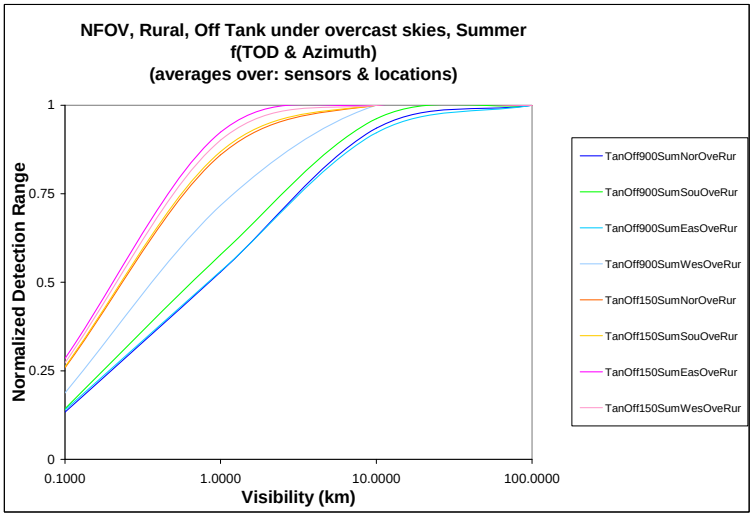


Figure C-12. Normalized detection range vs. visibility for a NFOV average sensor, in a rural aerosol, viewing an inactive tank under overcast skies in the summer, as a function of TOD, and azimuth. Averages were taken over locations, as presented in table C-2.

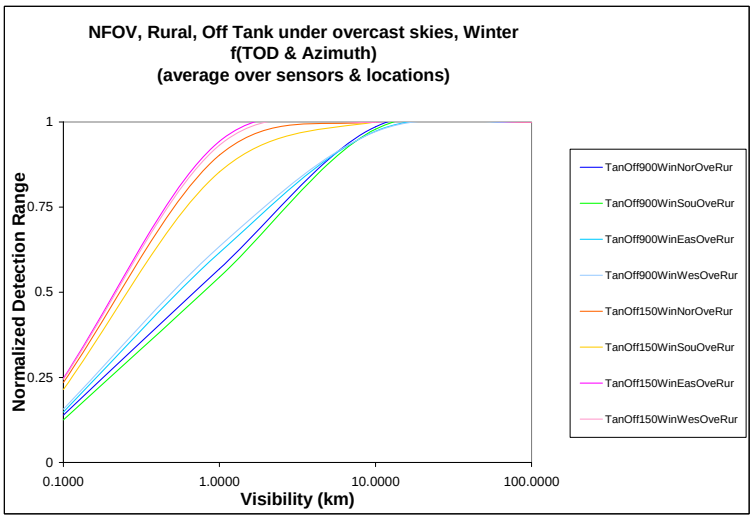


Figure C-13. Normalized detection range vs. visibility for a NFOV average sensor in a rural aerosol viewing an inactive tank under overcast skies in the winter as a function of TOD, and azimuth. Averages were taken over locations, as presented in table C-2.

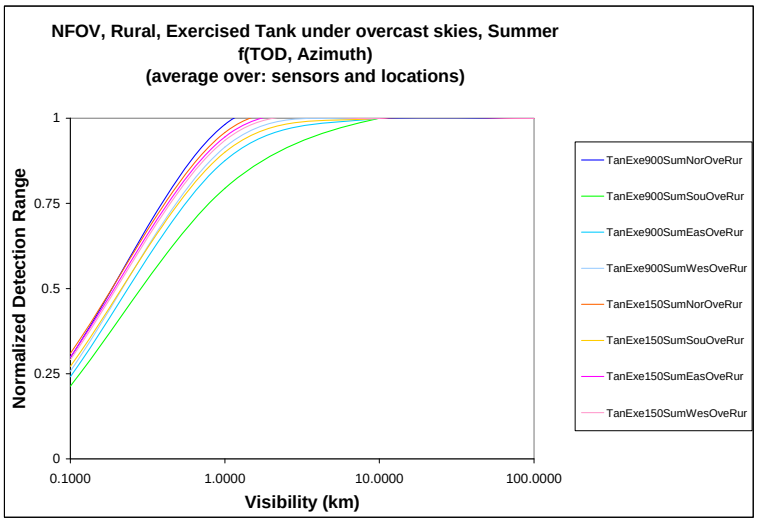


Figure C-14. Normalized detection range vs. visibility for a NFOV average sensor, in a rural aerosol, viewing an exercised tank under overcast skies in the summer, as a function of TOD, and azimuth. Averages were taken over locations, as presented in table C-2.

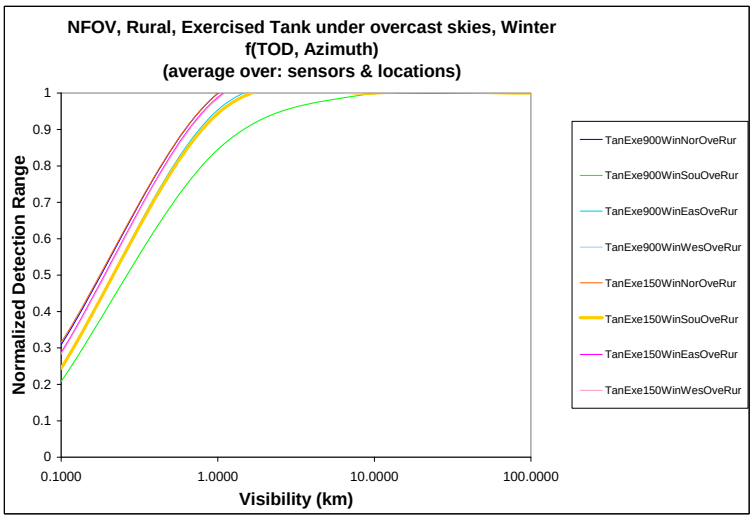


Figure C-15. Normalized detection range vs. visibility for a NFOV average sensor in a rural aerosol viewing an exercised tank under overcast skies in the winter as a function of TOD, and azimuth. Averages were taken over locations, as presented in table C-2.

## References


1. O'Brien, S. G.; Shirkey, R. C. *Adding Weather to Wargames*; ARL-TR-4005; U.S. Army Research Laboratory: White Sands Missile Range, NM, January 2007.

2. Press, W. H.; Teukolsky, S. A.; Vetterling, W. T.; Flannery, B. P. *Numerical Recipes in Fortran 77: the art of scientific computing*; 2nd ed, pp 678*ff*, Cambridge University Press: New York, NY, 2003.

| No. Copies | Organization |
|---|---|
| 1 | Army Research Laboratory<br>Attn: AMSRD-ARL-CI-EE (Dr. Hoock)<br>WSMR NM 88002-5501 |
| 2 | Army Research Laboratory<br>Attn: AMSRD-ARL-CI-EE (Dr. Shirkey)<br>WSMR NM 88002-5501 |
| 2 | Army Research Laboratory<br>Attn: AMSRD-ARL-CI-EE (Dr. O'Brien)<br>WSMR NM 88002-5501 |
| 1 | Director, USA TRADOC Analysis Center<br>Attn: ATRC-WEC (D. Durda)<br>WSMR, NM 88002-5502 |
| 1 | Army Research Laboratory<br>Attn: AMSRD-ARL-RO-EN (Dr. Bach)<br>PO Box 12211<br>Research Triangle Park, NC 27009 |
| 1 | Army Materiel Systems Analysis Activity<br>Attn: AMXSY-SC (J. Mazz)<br>392 Hopkins Road<br>APG MD 21005-5071 |
| 1 | Army Materiel Systems Analysis Activity<br>ATTN: AMSXY<br>APG MD 21005-5071 |
| 1 | Army Dugway Proving Ground<br>STEDP MT M<br>Attn: J. Bowers<br>Dugway UT 84022-5000 |
| 1 | USACE Engineer Research & Development Center<br>Cold Regions Research and Engineering Laboratory<br>Attn: Dr. Koenig<br>72 Lyme Road, Hanover, New Hampshire, USA 03755-1290 |
| 1 | Director, USA TRADOC Analysis Center<br>Attn: ATRC-W (P. Blechinger)<br>WSMR, NM 88002-5502 |
| 1 | Director, USA TRADOC Analysis Center<br>Attn: ATRC-WA (L. Southard)<br>WSMR, NM 88002-5502 |

| No. Copies | Organization |
|---|---|
| 1 | Director, USA TRADOC Analysis Center<br>Attn: ATRC-WEA (D. Mackey)<br>WSMR, NM 88002-5502 |
| 1 | Director, USA TRAC Anal Ctr<br>Attn: ATRC-FM (T. Bailey)<br>255 Sedgwick Ave<br>Ft Leavenworth, KS 66027-2345 |
| 1 | Director, USA TRAC Anal Ctr<br>Attn: ATRC-FMA (T. Gach)<br>255 Sedgwick Ave<br>Fort Leavenworth KS 66027-2345 |
| 1 | Director, USA TRAC Anal Ctr<br>Attn: ATRC-FMA (S. Glasgow)<br>255 Sedgwick Ave<br>Ft Leavenworth, KS 66027-2345 |
| 1 | United States Military Academy<br>Attn: Combat Simulation Laboratory<br>(Dr. P. West)<br>West Point, NY 10996 |
| 1 | Battle Command Simulation and Experimentation Directorate<br>Army Model and Simulation Division<br>Attn: DA G37 (DAMO-SBM)<br>400 Army Pentagon<br>Washington, DC 20310-0450 |
| 1 | USA PEO STRI<br>Attn: J. Blake<br>12350 Research Pkwy<br>Orlando, FL 32826-3276 |
| 1 | HQ USAFA/DFLIB<br>2354 Fairchild Drive, Suite 3A10<br>USAF Academy, CO 80840-6214 |
| 1 | HQ AFWA/DNX<br>106 Peacekeeper Dr STE 2N3<br>Offutt AFB NE 68113-4039 |
| 1 | Naval Research Laboratory<br>Attn: Dr. Goroch<br>Marine Meteorology Division, Code 7543<br>7 Grace Hopper Ave<br>Monterey, CA 93943-5006 |

| No. Copies | Organization |
|---|---|
| 1 | U.S. Naval War College<br>Attn: War Gaming Department (Code 33)<br>686 Cushing Road<br>Newport, Rhode Island 02841-1207 |
| 1 | Naval Weapons Surface Ctr<br>Attn: CODE G63<br>Dahlgren VA 22448-5000 |
| 1 | JWARS<br>Attn: C. Burdick<br>1555 Wilson Boulevard, Suite 619<br>Arlington, VA 22209 |
| 1 | Northrop Grumman Information Technology<br>Attn: Melanie Gouveia<br>100 Brickstone Square<br>Andover, MA 01810-5000 |
| 1 | Anteon Corp.<br>Attn: Mike Adams<br>46 Growing Rd<br>Hudson, NH 03051 |
| 1 | Northrop Grumman Corporation<br>Attn: R. Smith<br>E-10A BDT SEIT M&S IPT Lead<br>MS B06-222<br>2000 NASA Blvd<br>Melbourne, Florida 32907 |
| 1 | AFRL/IFOIL<br>525 Brooks Rd<br>Rome NY 13441-4505 |
| 1 | Tech Connect<br>AFRL/XPTC<br>Bldg 16, Rm 107<br>2275 D Street<br>WPAFB OH 45433-7226 |
| 1 | WSMR Technical Library<br>Attn: STEWS IM IT<br>WSMR NM 88002 |
| 1 | Technical Reports Boulder Laboratories Library<br>Attn: MC 5<br>325 Broadway<br>Boulder, CO 80305 |

| No. Copies | Organization |
|---|---|
| 1 | Ruth H. Hooker Research Library<br>4555 Overlook Ave, SW<br>Washington, DC 20375 |
| 1 | U.S. Army Research Laboratory<br>Attn: IMNE ALC IMS<br>Mail & Records Mgmt<br>Adelphi, MD 20783-1197 |
| 1 (ELEC) | Admnstr<br>Defns Techl Info Ctr<br>Attn: DTIC OCP (V Maddox)<br>8725 John J Kingman Rd., Ste. 0944<br>Ft Belvoir, VA 22060-6218 |
| 1 | U.S. Army Research Laboratory<br>Attn: AMSRD ARL CI OK TL Techl Lib<br>2800 Powder Mill Rd.<br>Adelphi, MD 20783-1197 |
| 1 | U.S. Army Research Laboratory<br>Attn: AMSRD ARL CI OK TP Techl Lib<br>APG, MD 21005 |

Total: 39 (1 Electronic, 38 CDs)

INTENTIONALLY LEFT BLANK.